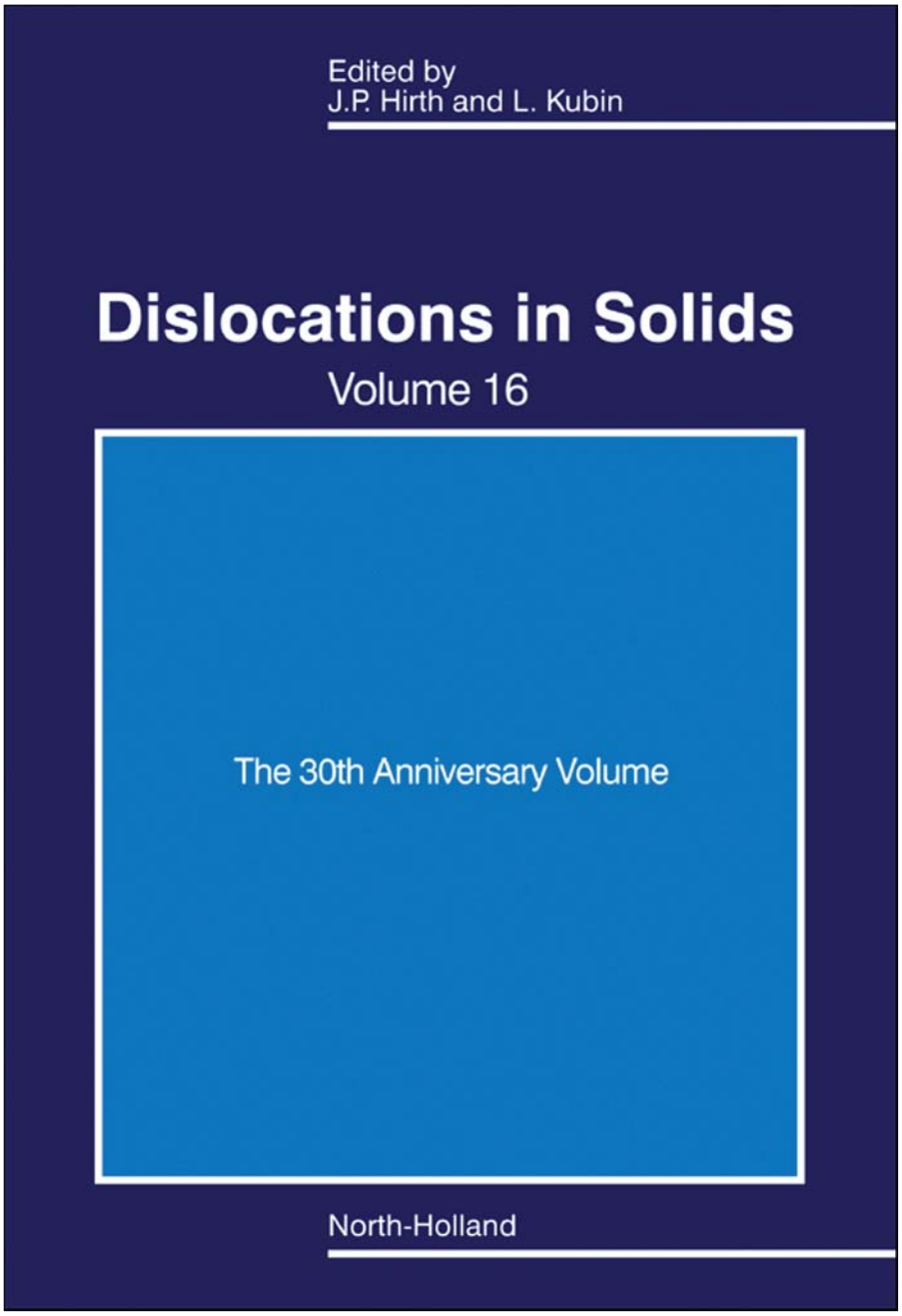

From J. Rabier, L. Pizzagalli, and J.L. Demenet, Dislocations in Silicon at High Stress. In: J. P. Hirth and L. Kubin, editors: Dislocations in Solids, Vol 16, Dislocations in Solids, J. P. Hirth and L. Kubin.
The Netherlands: North-Holland, 2010, pp. 47–108.
ISBN: 978-0-444-53443-9

CHAPTER 93

Dislocations in Silicon at High Stress

J. RABIER, L. PIZZAGALLI, AND J.L. DEMENET

PHYMAT, Université de Poitiers, CNRS UMR 6630, Boîte Postale 30179, F-86962 Futuroscope Chasseneuil Cedex, France

1572-4859, DOI: 10.1016/S1572-4859(09)01602-7

Dislocations in Solids
Edited by J. P. Hirth and L. Kubin

Contents

1. Introduction

The study of dislocations in semiconductors is strongly connected to the advent and development of the electronics industry. Indeed, it was very soon observed that the presence of crystalline defects, including dislocations, was detrimental to the processing and service life of devices. Thus, the very early research focused on the link between dislocation properties and their influence on the potential applications of semiconductors.

Silicon is obtained from silica, the main component of the Earth's crust; it was quickly used in electronics due to its natural abundance. As a consequence, many efforts were devoted to understanding the nature and properties of defects in this material. In addition, silicon appeared as, and is still nowadays, a model material for plasticity investigations because it is an elemental material with a crystal structure that is rather common among semiconducting materials. This material is also obtained as single crystals with zero dislocation content, which allows one to study dislocation nucleation.

This chapter aims at giving a comprehensive view about the structure and properties of dislocations obtained at high stress in silicon, which have been proved to have a different core structure from what was believed before.

Although many review papers or book chapters have been published on structures and properties of dislocation in semiconductors (see, e.g., [1–6]), the first part is devoted to present the context, ideas, and milestones that are necessary for understanding the subject of this chapter. The second part deals with the experimental works that have contributed to point out that different dislocation mechanisms and dislocation core structures are found at high stress in silicon: results of recent experiments are reported together with those of early experiments. These results, which reveal the existence of a different dislocation core structure at high stress, have promoted core structure analysis and numerous atomistic computations that are the subject of the third part. Finally, the results of experiments and computations are confronted in order to obtain a comprehensive view of the high-stress deformation regime existence. The transition between the two deformation regimes is also discussed.

1.1. Crystal structure and dislocations in silicon

Studies of the plasticity of semiconductors started at the beginning of the 1950s, with experiments on germanium and silicon, which were reported to be ductile above approximately 500 and 900 °C, respectively [7,8]. Seitz [8] explained Gallagher's measurements of plastic flow in germanium and silicon [7] in terms of

the theory of dislocations: the dislocations move by glide in {1 1 1} planes and have a Burgers vector equal to the ⟨1 1 0⟩-type translations in these planes. Besides, Seitz considered as improbable a dissociation of the dislocations into partials.

Shockley [9] was the first to describe the diamond-cubic structure of silicon and possible dislocations in this structure, followed by Hornstra [10], Haasen and Seeger [11], and Hirth and Lothe [12]. The structure is characterized by a tetrahedral environment of each atom. It can be represented as two face-centered cubic (fcc) sublattices shifted with respect to each other by a quarter of the ⟨1 1 1⟩ diagonal (Fig. 1).

Representing the atoms of one sublattice by capital letters and those of the other sublattice by small letters, one can describe the structure as an alternating stacking of close-packed layers of both types, …AaBbCcAaBbCc…. Fig. 2 shows a classical representation of the structure in projection along ⟨1 1 0⟩. In this figure, and by analogy with the fcc structure where the glide planes are {1 1 1} planes and the shortest translation vector of the lattice is 1/2⟨1 1 0⟩, there are two possible ways to produce a shear and, thus, for a dislocation to move (Fig. 2): between two widely spaced planes (e.g., Bb) of type I, or between two narrowly spaced planes (e.g., bC) of type II. Later, Hirth and Lothe [12] called these planes the shuffle set and the glide set, respectively. According to this terminology, which is still in use, dislocations lying on these planes are called shuffle dislocations and glide dislocations.

Hornstra [10] discussed several possible structures of dislocations in the diamond-cubic lattice. Starting from the fact that "an arbitrary direction in the crystal may be considered as the sum of steps in ⟨1 1 0⟩ directions," he considered that "the only simple dislocations that need to be studied are those along ⟨1 1 0⟩ directions." Then, it appears that the dislocation segments can be of type screw, edge, or 60° [Figs 3(a) and 3(b)].

Dash's observations [13] of Frank-Read sources in silicon, revealed by the copper decoration technique, showed that the dislocations have a pronounced tendency to

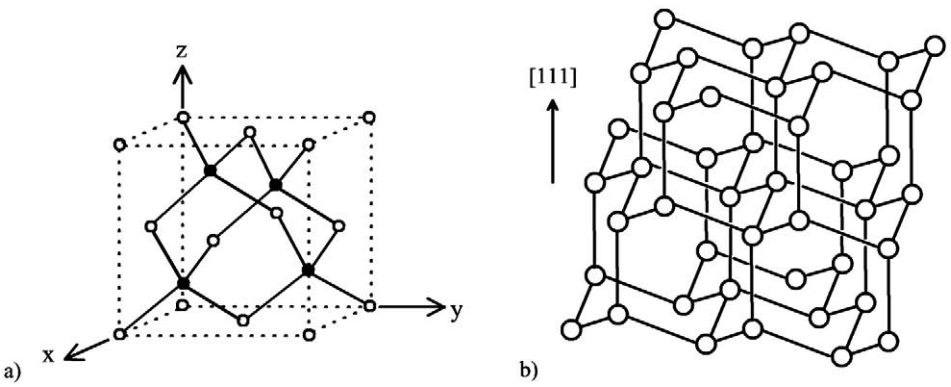

Fig. 1. The diamond structure. (a) The nodes of the two sublattices correspond to the white and black atoms, respectively and (b) view along ⟨1 1 0⟩.

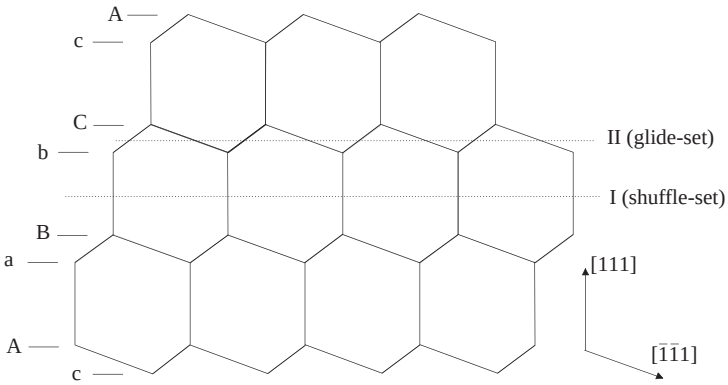

Fig. 2. The diamond structure viewed in projection along [1 $\bar{1}$ 0]. The (1 1 1) glide plane is horizontal, and the two possible shear locations I (shuffle set) and II (glide set) are indicated.

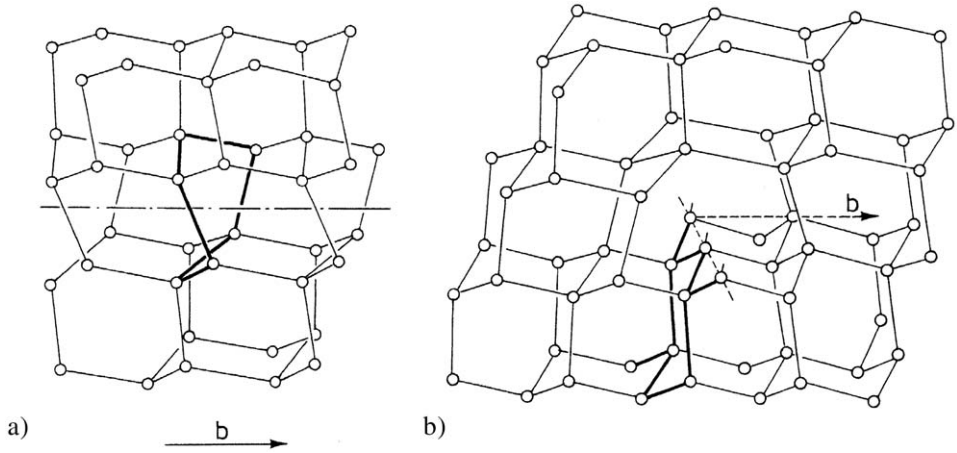

Fig. 3. Perfect dislocations in the diamond structure (after Hornstra [10]). (a) Screw dislocation and (b) 60° dislocation.

be predominantly of screw or 60° character. Later on (see, e.g., [1,14]), it was observed that, after a significant plastic deformation, dislocations are curved at high temperatures, but are aligned along the low-energy ⟨1 1 0⟩ directions when the temperature decreases and/or the stress increases.

Till the end of the 1960s, dislocations were thought to glide as perfect dislocations between the planes of type I (shuffle set). Indeed, the movement of a perfect dislocation in the shuffle set requires the breaking of one bond per atom, whereas three bonds must be broken in the glide set. In addition, the generally accepted view according to which shear is favored by a larger distance between slip planes is

consistent with a lower Peierls stress in the shuffle set and dislocations lying in this set.

1.2. The dissociation of dislocations

The dissociation of a perfect dislocation in its glide plane into partial dislocations of the 1/6⟨1 1 2⟩ Shockley-type was also an important domain of investigation. It was shown that the dissociation modes between two planes of type I or type II exhibit marked differences (Figs 4 and 5; see, e.g., Refs [12,15,16] for a detailed discussion). In short, the dissociation between planes of type II (glide set) leads to the formation of an intrinsic stacking fault and the distortions of the bonds remain confined in the cores of the partial dislocations. A glissile dissociation between planes of type I cannot be envisaged because the bonds between atoms in the stacking fault would be severely distorted.

Although the dissociation of a shuffle dislocation is unlikely *stricto sensu*, a dissociation involving shuffle dislocations was studied from a theoretical viewpoint by different authors [10–12,15]. This dissociation leads to a stacking fault between type II planes, bounded at one end by a glissile Shockley dislocation and at the

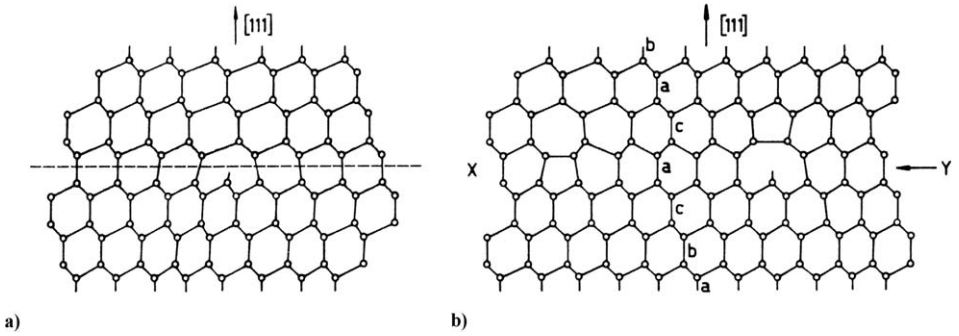

Fig. 4. 60° dislocation in the type I glide plane (shuffle set), after Amelinckx [16]. (a) Undissociated and (b) dissociated with formation of an intrinsic stacking fault. In that case, the stacking fault is of type II and is associated to a dislocation dipole at its right end (see Ref. [16]).

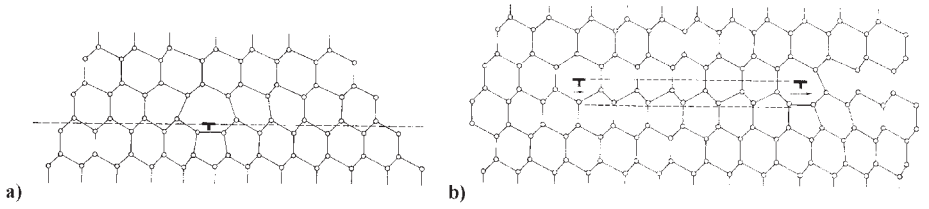

Fig. 5. 60° dislocation in the type II glide plane (glide set), after Amelinckx [16]. (a) Undissociated and (b) dissociated with formation of an intrinsic stacking fault.

other end by a sessile partial dislocation. The motion of this last partial requires a nonconservative atomic rearrangement. This type of rearrangement is called a shuffling and, for that reason, Hirth and Lothe [12] called the set of type I planes the shuffle set and the dislocations lying in these planes shuffle dislocations.

The dissociated shuffle dislocation, called ''extended shuffle dislocation'' by Alexander [1], can be described in two ways: either as a stacking-fault ribbon bounded by two Shockley dislocations of opposite sign associated with a shuffle dislocation, or as a dissociated glide (DG) dislocation that has emitted or absorbed a line of vacancies or interstitials in the core of one of its partials.

An essential contribution to the knowledge of dislocation cores in semiconductors was brought by the weak-beam technique, which was developed by the end of the 1960s (see Refs [17–19] for the case of Si). This transmission electron microscopy (TEM) technique allowed obtaining a finer image of the region of the crystal close to the actual position of dislocations. In silicon, the dislocations generated by deformation at 850 and 1200 °C were found to be dissociated in the (1 1 1) plane according to the reaction:

$$\frac{a}{2}[1\,\bar{1}\,0] \rightarrow \frac{a}{6}[2\,\bar{1}\,\bar{1}] + \frac{a}{6}[1\,\bar{2}\,1] \tag{1}$$

These observations confirmed previous observations of extended nodes in silicon made by Aerts et al. [20]. Dislocation dissociation was also observed in germanium using the same technique [19]. Later, Meingast and Alexander [21], showed that dislocations also moved in dissociated form in germanium thin foils locally heated in the electron microscope. Regarding the $\langle 1\,1\,0 \rangle$ low-energy directions, the perfect screw dislocation is dissociated into two 30° partial dislocations, and the 60° perfect dislocation is dissociated into a 30° partial dislocation and a 90° partial dislocation (Fig. 6).

From the observation of the dissociation of dislocations, both at rest and moving, it was concluded that dissociated dislocations belong to the glide set. In principle, TEM examinations of edge-on dislocation lines at high resolution and of the associated simulated contrasts should allow one to distinguish the dissociation modes.

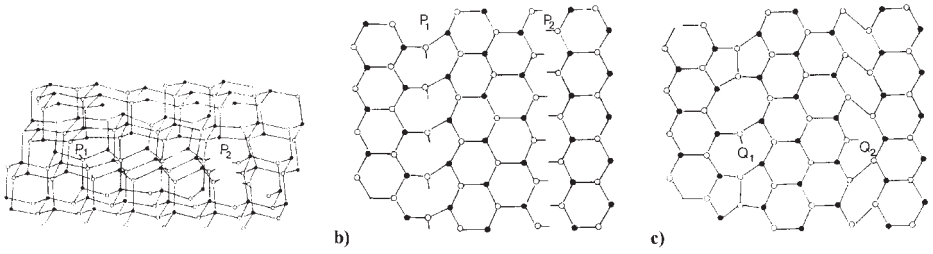

Fig. 6. (a) A 60° dislocation dissociated in the glide set into 30° (P_1) and 90° (P_2) partial dislocations. (b) Same configuration projected on the (1 1 1) glide plane. Partial dislocations are not reconstructed. (c) Partial dislocations are reconstructed. A reconstruction defect (soliton) is shown on each partial. After George and Rabier [2].

In practice, the occurrence of defects along the dislocation lines (kinks, jogs, point defects, …) makes the interpretation of high-resolution micrographs difficult and hazardous.

Although most of the dislocations are seen to be dissociated at the scale of transmission electron microscopy, constrictions were also observed on dislocation segments in silicon [19] as well as in germanium [22,23]. These constrictions are particularly numerous after high-temperature deformation, around 520 °C for germanium and 800 °C for silicon. Packeiser and Haasen [22,23] showed, in germanium, that they are formed on jogs with a height larger than the spacing between glide planes. The same explanation could apply to silicon. A link between point defects and local modifications of dislocation splitting observed by TEM was suggested in order to explain that jogs were able to move along the dislocation lines. They were assumed to do so by an exchange of point defects between the dislocation and the lattice [1]. Moreover, it was not excluded that these constricted segments could belong to the shuffle set [15]. This can be related to the work of Louchet and Thibault-Desseaux [24], who discussed the possible coexistence of glide and shuffle partial dislocations. These authors considered that dissociation is not restricted to the glide set and that the core structure is not unique along a given partial. Partial dislocations have complex cores with an average glide character but they contain a number of shuffle sites due to point defects, the nature of which depends on the character of the dislocations.

1.3. Bond reconstruction in the dislocation cores

The possible occurrence of bond reconstruction in the dislocation cores became quickly an open issue, in particular for researchers working in the electronics industry. Shockley [9] was the first to notice that the unsaturated bonds appearing at edge dislocation cores in semiconductors could form a one-dimensional energy band partially filled with electrons. After this seminal work, other authors showed that acceptor and recombination centers were introduced during plastic deformation. This effect was presumably connected to dangling bonds present in dislocation cores, the carrier lifetime being inversely proportional to the dislocation density. For more details, the reader is referred to a recent and well-documented historical summary published by Figielski [5] on dislocations considered as electrically active centers. At the same time microstructural studies were devoted to electrical and optical properties of dislocations, using different techniques like electronic paramagnetic resonance (EPR), deep level transient spectroscopy (DLTS), electron beam induced current (EBIC), and photo- or cathodo-luminescence. The influence of dislocations on electrical properties, namely the density, mobility, and lifetime of electrical carriers was studied as a subject of basic research as well as a critical point to obtain reliable devices.

Most of these studies were performed on samples deformed between 650 and 850 °C, which are temperatures easily accessible in laboratory and for which silicon still presents some ductility. The Alexander group in Köln [25,26] and the Ossipyan

group in Chernogolovka [27] investigated the dislocation cores using EPR. Indeed, this technique is sensitive to unpaired electrons in the core of dislocations and thus to the presence of dangling bonds. EPR spectra are different according to the deformation temperature between 850 and 420 °C, and more resonance peaks are observed at high temperature. However, the existence of a recombination center not associated with a particular type of dislocation seemed to indicate that the movement of dislocations is correlated with the existence of point defects in the dislocation cores. This point is still a matter of debate, and it is not clear whether point defects are dragged by dislocations during their motion or left behind by the dislocations. The recent observation of dislocation trails revealed by selective chemical etching and possibly associated with EBIC and DLTS signals stirred up a renewal of interest to this question [28]. Besides, EPR experiments showed that the number of dangling bonds is small as compared to the number of sites on the dislocation line, less than 5%. Thus, most of the dislocations should be reconstructed.

Because of the strong covalent bonding, one can imagine that relaxation involving bond rearrangements can occur and dislocation cores should be reconstructed. A 60° dislocation dissociates into 30° and 90° partials with dangling bonds almost parallel to the slip plane [Figs 6(a) and 6(b)]. Those dangling bonds may disappear pairwise by core reconstruction. The calculations of reconstructed core structures in silicon were essentially made on the 30° and 90° partials. The full reconstruction of a 30° partial leads to the unique possibility of a double-period (DP) core [Fig. 6(c)]. On the other hand, a 90° partial can be reconstructed in two ways, leading to a single-period (SP) core [Fig. 6(c)] or a DP core. The SP reconstruction was independently proposed by Hirsch [29] and Jones [30], and further discussed by Bennetto et al. [31]. The DP reconstruction proposed in Ref. [31] doubles the period along the dislocation line. Calculations using various approaches and potentials slightly favor this DP core reconstruction [32]. However, the occurrence of defects along the dislocation line (impurities, reconstruction defects, or solitons, vacancies, interstitials, …) could affect locally the reconstruction mechanism. Energy values associated to these defects were calculated and can be found in Ref. [32].

1.4. Dislocation mobility

The mobility of the dislocations was for a long time another important theoretical and experimental topic. Dislocation motion can be assisted by temperature and the external stress. The critical stress for the movement of a dislocation at 0 K is defined as the Peierls stress. At finite temperatures, the motion of a dislocation from a low-energy valley to the next one occurs by the local nucleation of short segments, the kink pairs, which cross the energy barrier in the direction of dislocation motion. Then, each kink propagates sideways along the dislocation line, which transfers the latter as a whole into the neighboring low-energy valley. These two elementary mechanisms are associated with an energy barrier. The energy necessary to

overcome a Peierls potential of the first kind and nucleate a kink pair is $2F_k$, where F_k is the formation energy of a single kink. W_m, the migration energy, is the energy to overcome the Peierls potential of the second kind, which allows a kink to propagate along the line. Contrary to ''usual'' fcc metals, where W_m is negligible, both energies could be high and of the same order in semiconductors. These mechanisms of kink pair nucleation and kink migration were studied by Hirth and Lothe [12] in crystals with a high Peierls relief, taking into account the number of nucleation sites and the length of the free segments. The mean free path of a kink along the dislocation line is limited by the presence of another kink of opposite sign, with which it annihilates, or by the presence of a pinning obstacle. In steady-state conditions, a dislocation moves with a constant velocity, which implies that each pinning or annihilation event is compensated by a nucleation event. This kink-diffusion model leads to two regimes: a regime where the dislocation velocity depends on the length of segments because the kink can propagate all along the line, and a regime where the dislocation velocity is independent from the length of segments because of the kink–kink collisions.

The reconstruction of core bonds leads to the existence of various types of kinks according to the nature of the partial (30° or 90°) and the position of the kink, at the right or left side of its companion. The different types of kinks were classified and analyzed by atomistic simulations for determining their energy and their probability of occurrence. In the case of a 90° partial, the unreconstructed configuration is symmetric and both right and left kinks are identical. Due to the reconstructed nature of the dislocation core, many different topological kinks can be formed. In the case of the 30° partial the number of reconstructed kinks is even more important since, there are two different kink structures in the unreconstructed configuration due to the intrinsic left–right asymmetry of a kink pair [33].

The partial reconstruction of bonds can occur along the line as well as at a kink, leading to the existence of reconstruction defects, or solitons, as mentioned above. The formation of these reconstruction defects is thermically activated and their low migration energy makes them highly mobile. This description is the basis of the model initially proposed by Jones [34] and Heggie and Jones [35], which was further developed by Bulatov et al. [33]. Solitons facilitate the nucleation and the migration of the kink pairs by locally restoring the covalent bonding. Within the framework of this model, it seems reasonable to think that the energies associated to the first and second kinds of Peierls potentials are of the same order.

Attempts to determine experimentally the values of F_k and W_m were carried out using various techniques: internal friction [36,37], deformation under load pulse sequence [38], and TEM. There are very few internal friction experiments on semiconductors. The reason is the brittleness of these materials and the need to work at very low frequencies in order to get a relaxation peak at moderate temperatures. The direct observation of kink motion was realized by TEM, either by studying the relaxation of out-of-equilibrium dissociated dislocations [39], by *in situ* deformation [40], or by using forbidden reflections in the high-resolution mode [41,42]. These various experiments were analyzed within the framework of the kink-diffusion model of Hirth and Lothe [12], which does not take into account

the dissociation of the dislocations. The applied stress can lead to different Peach–Koehler forces on the partials, so that the dissociation width depends on the applied stress. Thus, under low stresses, the nucleation of kink pairs on both partials can be correlated. Using atomic-resolution electron microscopy, Kolar et al. [42] analyzed recordings of kinks moving on partial dislocations and obtained the values $F_k = 0.73\,\text{eV}$ and $W_m = 1.24\,\text{eV}$ at 600 °C. The various results obtained by different techniques show that, in contrast to the case of metals, the Peierls potential of the second kind is important with a value of W_m around 1.2 eV. This is in agreement with the first calculations of Jones [43]. The Hirth and Lothe model predicts the occurrence of a transition between the length-dependent and the kink-collision regimes characterized by a change in the kink formation energy. The two regimes of kink motion were observed by TEM [39,40], with a critical segment length of about 0.4 μm at the transition, but without any change in activation energy. The entropy term contribution, which is not taken into account in the model, should exhibit unrealistically high values to yield a good agreement between theory and experiment. It appears, thus, that the length-independent regime found experimentally should not be a kink-collision regime. This is also supported by other experimental results obtained by intermittent pulse loading [38] or by monitoring the motion of a threading dislocation in strained thin films [44]. Then, kink motion may be limited by obstacles like point defects along the dislocation lines.

The dislocation velocities can also be measured on macroscopic specimens. Double etch pits and X-ray topography are the most common techniques used for this purpose. The dislocation velocities v were measured by different authors as a function of temperature T and stress τ; the results were analyzed using the phenomenological law:

$$v = v_0 \left(\frac{\tau}{\tau_0}\right)^m \exp\left(-\frac{Q}{kT}\right), \tag{2}$$

where v_0 and τ_0 are constants, k is the Boltzmann's constant, the exponent m is usually between 1 and 2, and Q is the total activation energy. In the most explored range of intermediate stress and temperature values, 1–50 MPa and 600–800 °C, respectively, experimental results on pure silicon lead to $m = 1$ and $Q \sim 2.2\,\text{eV}$. This seems to confirm that only one of the two predicted regimes is observed.

To summarize this brief history of dislocations in silicon, it appears that some points are well established. In particular, at high and medium temperatures, which are the best documented domains, dislocations lie in the glide set where they are dissociated both at rest and when they move. They have to overcome high Peierls potentials of the first and second kinds. However, several questions remain a matter of debate: what is the mean free path of kinks? What is the density of localized obstacles along the dislocation lines? What is the role of point defects on dislocation mobility?

In 1996, Duesbery and Joós [45] determined that in "usual stress conditions," dislocations should belong to the glide set. Using Peierls barriers deduced from atomistic computations, these authors calculated the kink pair activation energies

for perfect shuffle (PS) screw dislocations and for the 30° glide partial. The activation energy for screw shuffle dislocations was the highest in the whole stress range, but the difference was found to decrease with increasing stress. Extrapolating these results to high stresses, it was predicted that a transition should occur from plastic deformation carried out by glide dislocations to plastic deformation carried out by shuffle dislocations around $\tau/\mu = 0.01$ (μ is the shear modulus). This has constituted the motivation for revisiting the plastic deformation of silicon at high stress, both experimentally and theoretically. The results of these investigations are described in the following parts of this chapter.

2. High-stress deformation: experimental features

Low-temperature high-stress deformation tests in silicon allowed investigating extreme mechanical conditions such as those encountered in the machining of wafers, in deformation regimes controlled by decorrelated partial motion or mechanical twinning, and in the deformation mechanisms involved in the brittle to ductile transition (BDT). The effect of electronic doping was also investigated, since it is expected to be more important when the deformation temperature is low. Indeed, the BDT temperature was found to depend on doping, in good agreement with the dependence of dislocation velocities on dopant concentration [46,47]. Furthermore, renewed interest on high-stress deformation mechanisms was stimulated in the last decade by investigations of the plastic properties of nanostructured materials. These small-scale objects exhibit a high strength that is due to size effects. For example, it was shown that silicon nanopillars could sustain stresses that are much higher than the ones encountered in bulk materials at the BDT [48]. In this context, understanding the nucleation of dislocations as well as the elementary deformation mechanisms at high stress not only is a challenge in defects physics but becomes a critical issue for nanostructural engineering.

In order to achieve such high stresses in low temperature deformation regimes, two main techniques can be used, which superimpose a hydrostatic component to an applied shear stress: microindentation and deformation under a confining pressure. The hydrostatic component limits cracks extension and induces a shift in the BDT toward low temperatures. Microindentation (or nanoindentation) tests are very easy to perform but they suffer from two main drawbacks: the stress tensor is not known and the plastic region is confined to a very small volume of the specimen, which makes TEM observations of the deformation substructure quite difficult.

Deformation under hydrostatic pressure is less easy to carry out, but it allows one to perform TEM observations in larger areas. Although the hydrostatic pressure can be controlled quite accurately, the main drawback – that depends on the experimental setup – can be the measurement of the uniaxial stress. In the range of pressures suited for studying the plasticity of silicon, this problem can now be solved using deformation apparatuses devised to function in synchrotron beamlines (see Section 2.3.2).

In what follows, we report on experiments on the deformation of silicon, which were designed to shed light into the main features of high-stress dislocation mechanisms.

2.1. Deformation experiments at high stress

2.1.1. Dislocation microstructures after indentation

Indentation techniques were widely used for a long time to investigate the plasticity of silicon at low temperature. However, a difficulty arises because silicon shows a phase transition from diamond-cubic structure to β-Sn metallic Si at a pressure of about 12 GPa [49]. As the shear stress increases during an indentation test, the hydrostatic component simultaneously increases and the critical pressure for the phase transition can be reached. In such conditions, the hardness values and dislocation microstructures cannot be representative of dislocation-induced plasticity mechanisms. Indeed, the occurrence of the phase transition under indentation was found to explain the observed saturation of hardness values below 400 °C ([50,51]; see also Fig. 8). Dislocations were nevertheless observed after indentation at temperatures lower than 400 °C, but their possible connection with the phase transition was not investigated.

After indentation at room temperature, dislocations are not mobile and stay in the close vicinity of the indentation site. This results in a very high local density of dislocations, which are difficult to resolve individually [52,53]. For that reason, most of the observations of dislocations were performed after indentation at a medium temperature or after a room temperature anneal of the microstructure, in order to promote dislocation nucleation or the propagation of the dislocations at some distance from the imprints (see, e.g., [52]). After anneals at typically 400 °C, the dislocation configurations are similar to the ones found in usual conditions, that is, dislocations with $\langle 1\,1\,0 \rangle$ Burgers vectors, $\{1\,1\,1\}$ glide planes, and glide dislocation loops exhibiting a hexagonal shape with segments lying along the $\langle 1\,1\,0 \rangle$ directions. In one of the many works performed on silicon indentation, Hill and Rowcliffe [53] were able to derive original results from the observation of dislocations after indentation at room temperature and at 300 °C. These authors noticed that "indentation at room temperature produces shear loops composed of long 30° dislocations and short 60° dislocations segments." Specimens indented at 300 °C contained the same type of dislocations but the 30° dislocations were not straight anymore. Hill and Rowcliffe [53] concluded that the types of dislocations and their arrangements differ considerably from those observed in silicon at elevated temperature. They proposed a mechanism in which the theoretical shear strength being locally exceeded, the dislocations resulted from the accommodation of displacements by non-dislocation-mediated block slip.

2.1.2. High-stress plastic deformation under a confining pressure up to 1.5 GPa

The first work on the deformation of silicon under hydrostatic pressure as a way to reach high stresses was performed by Castaing et al. [54], using a Griggs apparatus

dedicated to the deformation of minerals under pressure. In this experimental setup, confining pressures are produced by a solid confining medium. The accuracy of applied stress measurements suffers from the friction stress exerted by the solid confining medium on the moving deformation rams. Single crystals of silicon with ⟨1 2 3⟩ (oriented for single slip) and ⟨1 0 0⟩ compression axes were deformed under a pressure of 1.5 GPa between 450 and 275 °C at imposed strain rates ranging from 2×10^{-5} to $2 \times 10^{-6}\,s^{-1}$. Without prestrain, the lowest temperature at which plastic deformation occurred under a strain rate of $2 \times 10^{-6}\,s^{-1}$ was 450 °C. At the same strain rate and after a prestrain at 450 °C, the lowest temperature at which macroscopic plasticity could be obtained was 275 °C.

Fig. 7 shows a stress–strain curve obtained at low temperature on a virgin silicon crystal [54,55]. The yield point usually found at medium temperatures is still present. This behavior is characteristic of a low initial dislocation density followed by a multiplication stage and an overshoot of the dislocation density after the multiplication stage.

The temperature dependence of the yield stress was analyzed using the rate equation:

$$\dot{\gamma} = \dot{\gamma}_0 \exp\left(-\frac{\Delta G}{kT}\right), \tag{3}$$

where $\dot{\gamma}$ and $\dot{\gamma}_0$ are, respectively, the resolved imposed strain rate and a reference strain rate. The stress dependence of the activation free energy was determined by stress relaxation tests and was found to be logarithmic. The temperature dependence of the yield stress can then be written in the form:

$$\ln(\tau) = \ln(\tau_0) + \beta T, \tag{4}$$

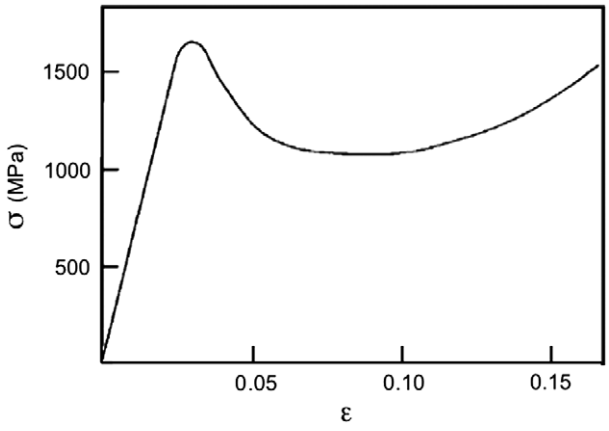

Fig. 7. Stress–strain curve of a ⟨1 2 3⟩ Si crystal deformed at $T = 425$ °C under a strain rate of $2 \times 10^{-6}\,s^{-1}$ and a confining pressure of 700 MPa. After Demenet [55].

where the strain rate dependence is accounted for by the coefficient β. The flow stress extrapolated at 0 K, τ_0, is between 100 and 200 GPa, that is, it is comparable to the shear modulus. A large value was found for the ratio $\Delta G/kT = c$ ($c = 36$); this value is surprising since c should in principle lie between 20 and 30 [56]. These two unexpected experimental results imply that either the above analysis is questionable or there are several controlling deformation mechanisms in the small temperature interval investigated (250–450 °C).

The temperature dependence of the yield stress obtained in Si down to 275 °C was compared with microhardness data obtained down to room temperature (Fig. 8) [51]. In contrast to microhardness data, the yield stress values do not level off below 400 °C, which is consistent with the occurrence under the microindenter of the phase transition mentioned in Section 2.1.1 [50,52]. In the compression tests, the pressure was kept below the critical value for the onset of this transition.

The temperature dependencies of the yield stresses are similar for samples deformed along the ⟨1 2 3⟩ and ⟨1 0 0⟩ compression axes [54,55,58]. However, the deformation microstructures look very different. This feature is related to the resolved applied stresses on the active slip planes. These stresses are such that, for dissociated glide dislocations, they increase the dissociation width for the ⟨1 2 3⟩ loading axis and decrease it for the ⟨1 0 0⟩ loading axis.

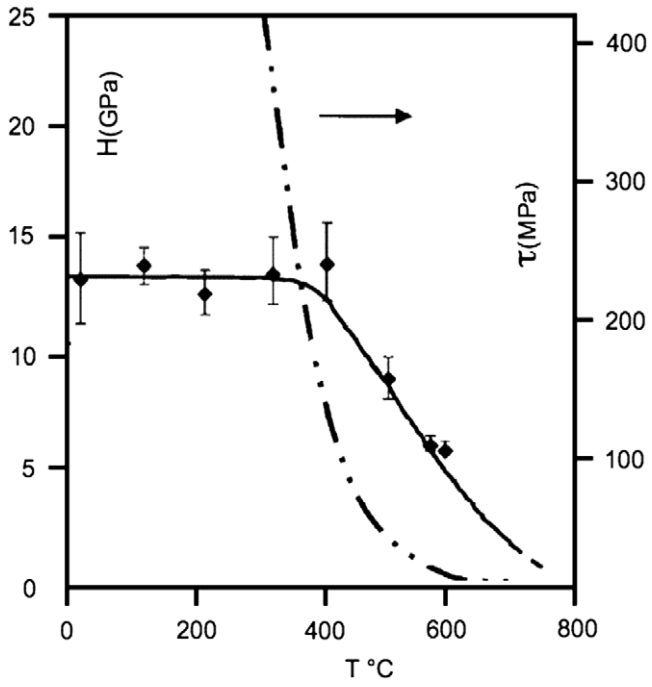

Fig. 8. Hardness (H) as a function of temperature (from Suzuki and Ohmura [51]). The temperature dependence of the yield stress is also schematically drawn (from Castaing et al. [54]). After Rabier and Demenet [57].

Fig. 9(a) shows the microstructure obtained after deformation of a ⟨1 2 3⟩ sample; when observed in the primary glide plane, it consists of dissociated dislocations. There is a tendency for the screw segments to be longer than the other ones. However, this microstructure is not very different from what is found at higher temperatures under standard deformation conditions. Moreover, although the stress tensor favors the narrowing of the stacking fault, no perfect dislocations are obtained. The deformation microstructure of samples deformed along the ⟨1 0 0⟩ compression axis is quite different. It consists of extended stacking faults that point at a deformation mechanism controlled by the movement of decorrelated partials [Fig. 9(b)].

Although the deformation microstructures are different in these two orientations, the analysis of surface source nucleation mechanisms in silicon led to the conclusion that the activation energies for the movement of decorrelated partials and of dissociated dislocations should be the same at high stresses, in agreement with the apparent macroscopic response [57].

These experiments under hydrostatic pressure allowed the study of silicon plasticity under high stresses in the absence of a phase transition. However, although stresses as high as 2 GPa were reached in the plastic regime, the dislocation microstructures were not found to significantly differ from those found in usual low-stress deformation conditions where dissociated dislocations control plasticity. This may relate to the prestrain that was needed to increase substantially the range of experimental conditions leading to plastic behavior (see Ref. [57] for more detail and discussion).

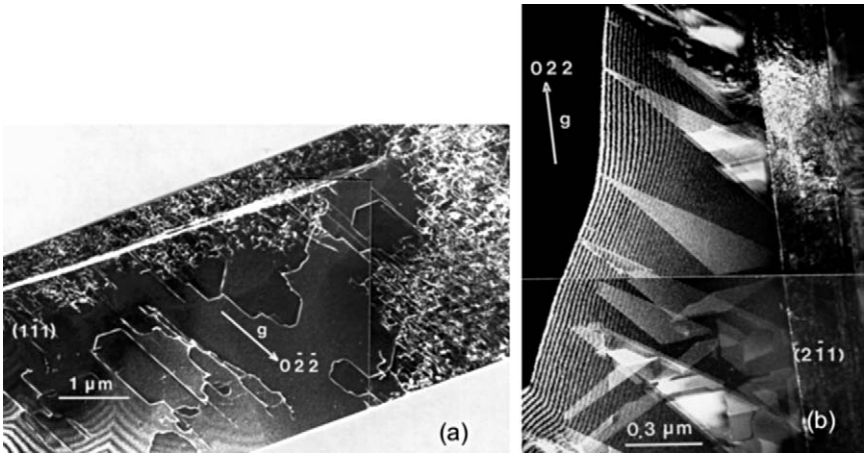

Fig. 9. Dislocation microstructures in silicon crystals after high-stress deformation. (a) ⟨1 2 3⟩ crystal deformed up to the upper yield stress ($\tau = 800$ MPa) at $T = 425\,^{\circ}$C under a strain rate of $2 \times 10^{-6}\,s^{-1}$ and a confining pressure of 700 MPa (after Demenet [55]). (b) ⟨1 0 0⟩ crystal deformed at $T = 450\,^{\circ}$C under a strain rate of $2 \times 10^{-6}\,s^{-1}$ and a confining pressure of 1.5 GPa (after Castaing et al. [54]).

2.2. Evidence of the nucleation of perfect dislocations at high stresses

2.2.1. Plastic deformation under 5 GPa

In order to obtain plasticity at lower temperatures and larger yield stresses, an increase of the confining pressure is required, especially for dislocation-free materials. Yet, the confining pressure has to be maintained below 12 GPa in order to avoid the phase transition artefacts encountered during indentation below 400 °C (Section 2.1.2). Since the highest pressure that can be achieved with a standard Griggs apparatus is 1.5 GPa, experiments at higher pressures require another deformation setting that is routinely used in the field of geophysics: the multi-anvil apparatus. This deformation machine makes it possible to apply pressures up to 25 GPa on ''large'' volumes of materials, but in this type of experiments the yield stress cannot be measured during the mechanical test. A multi-anvil apparatus dedicated to plastic deformation, in which the confining medium was designed to produce an additional uniaxial stress during pressure application [59], was used by Rabier et al. [60,61] to deform virgin Si single crystals. Plastic deformation could be obtained under a hydrostatic pressure of 5 GPa at temperatures as low as room temperature and 150 °C. The applied pressure around the sample was raised at a rate of 1 GPa/h. As a consequence of the design of the solid confining medium, a uniaxial stress also builds up during the pressure application. In such conditions, the deformation rate can be roughly estimated to be $5 \times 10^{-5}\,s^{-1}$ and a permanent strain of several percent is obtained in these tests.

The analysis of the deformed samples shows that the macroscopic deformation results from crack generation as well as from dislocation nucleation and motion. TEM investigations of the deformation microstructure show dislocations that were nucleated at the lateral surfaces of cracks and others that propagated in the bulk material and accumulated in areas with very high dislocation densities. The dislocation loops emitted from the crack surfaces are elongated along specific crystallographic directions [Fig. 10(a)] and so are the dislocation loops that

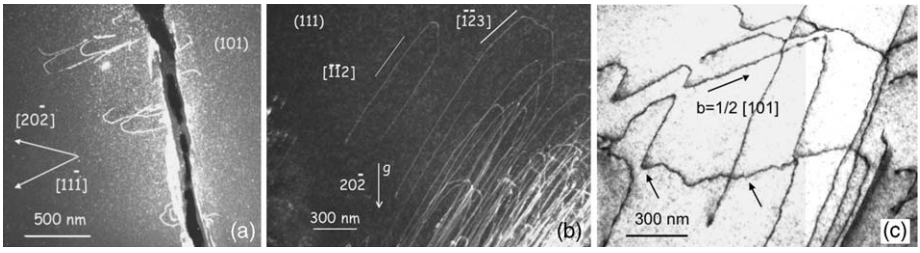

Fig. 10. Deformation microstructures containing perfect dislocations (the confining pressure is 5 GPa). (a) Deformation temperature: $T = 293$ °C; (1 0 1) foil plane, weak-beam dark field ($4.1g$, $g = 2\,0\,\bar{2}$). The dislocations nucleated at crack edges are of $1/2[1\,0\,\bar{1}](1\,\bar{1}\,1)$ type. These half-loops are elongated along the [3 2 1] direction (after Rabier and Demenet [62]). (b) In the bulk, the same dislocations tend to be aligned along several Peierls valleys: $\langle 1\,1\,2\rangle/30°$, $\langle 1\,2\,3\rangle/41°$, and screw orientation (after Rabier et al. [62]). (c) Deformation temperature: $T = 150$ °C. Same Peierls valleys as at room temperature; some strong pinning points are indicated by arrows (after Rabier et al. [61]).

propagated in the bulk of the sample [Fig. 10(b)]. Strong pinning points are evidenced together with wavy, unstable orientations that result from the presence of very short segments with different orientations [Fig. 10(c)]. Weak-beam dark field contrast studies revealed, that these dislocations are perfect dislocations with the usual 1/2⟨1 1 0⟩ Burgers vectors and {1 1 1} glide planes. The straight segments were found to lie along the screw orientation, as well as along ⟨1 1 2⟩/30° and ⟨1 2 3⟩/41° which can be assumed to be Peierls valleys. These Peierls valley directions were not reported before and differ from the usual ⟨1 1 0⟩ ones that characterize dissociated glide dislocations. The density of pinning points was found to be the largest at the deformation temperature of 150 °C [Fig. 10(c)].

These observations were made in samples deformed in compression along the ⟨1 2 3⟩ orientation, for which one usually finds dissociated glide dislocations with a small dissociation width (Section 2.1.2). In order to confirm the occurrence of perfect dislocations, a compression axis with a ⟨1 0 0⟩ orientation was selected to check whether or not extended stacking faults are nucleated under large stresses. In contrast to what is found at higher deformation temperatures (Section 2.1.2), extended stacking faults were not evidenced. Instead, the microstructure was of same type as in the ⟨1 2 3⟩ samples and contained perfect dislocations. This result confirmed the occurrence of a new deformation mechanism involving perfect dislocations, in a stress range where dissociated glide dislocations would no longer have a stable, finite dissociation width. Owing to the apparently perfect nature of the dislocations, cross slip is expected to be an efficient relaxation mechanism. Evidence of this mechanism was looked for in TEM samples, but, surprisingly, it was quite difficult to find any trace of cross slip at this scale of observation.

In this context, various high-stress deformation conditions were tested, with the aim of producing other deformation microstructures containing perfect dislocations. The results are discussed in the next section.

2.2.2. Plastic deformation in the metallic phase

Since a phase transformation as well as dislocations can be evidenced simultaneously after indentation tests at room temperature, the deformation of silicon under a pressure of 15 GPa, that is, in the β-Sn metallic phase, was investigated at 293 K using the same device as in previous tests [62]. In such conditions, silicon deformed along ⟨1 0 0⟩ showed an exceptional ductility: a macroscopic strain of more than 20% was obtained without major failure. The *postmortem* observations showed silicon high-pressure phases (Si III, Si XII). These phases were characterized by their Raman spectra on the surfaces of sections extracted from the specimen (unpublished) and by TEM on grains of the different phases. No amorphous phase was evidenced. In addition to these high-pressure phases, a large fraction of the specimen recovered the diamond-cubic phase Si I after the deformation test. TEM observations of this recovered phase showed evidence for an intense plastic activity. Perfect dislocations were found, emerging from dense glide bands, as well as isolated defects in less dislocation-dense areas [Figs 11(a) and 11(b)]. Deformation bands containing mechanical twins were also evidenced (J. Rabier et al., unpublished data). The characteristic features of isolated

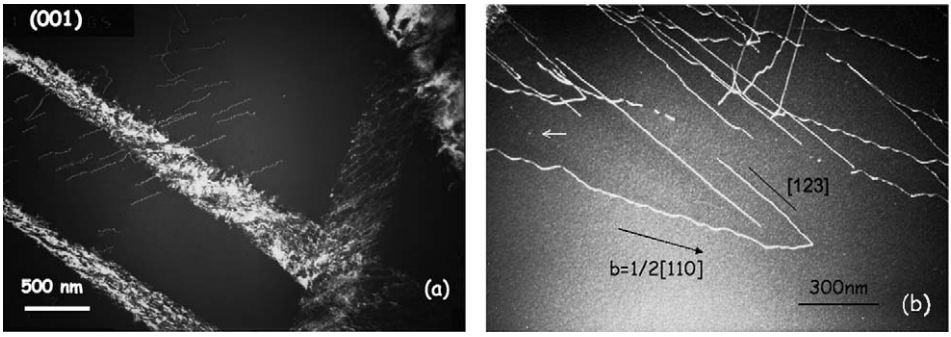

Fig. 11. Silicon deformed in the metallic phase (confining pressure: 15 GPa, $T = 293\,^{\circ}C$). Deformation microstrutures in the diamond-cubic Si I phase. (a) Glide bands with a high dislocation density and isolated perfect dislocations. Weak-beam dark field $2g$, $g = 0\,4\,0$. (b) Isolated perfect dislocations with $\langle 1\,2\,3\rangle/41^{\circ}$ orientation (straight lines) and unstable 1/2[1 1 0] screw segments. After Rabier et al. [62].

dislocations escaping from dense dislocation bands were investigated [62]. The dislocation lines contained segments with average screw orientation and $\langle 1\,2\,3\rangle/41^{\circ}$ segments. The screw orientation appeared to be unstable and was composed of $\langle 1\,2\,3\rangle/41^{\circ}$ segments. Segmented small loops built up with these segments were found to result from dislocation dipole annihilations [62].

2.2.3. *Dislocation microstructure resulting from surface scratches*

Scratching at room temperature followed by annealing at about 800 °C under a bending stress was widely used to nucleate dislocations in silicon. As an example, small densities of large dislocation loops suited for X-ray topography observations could be produced by this method in order to study dislocation mobility as a function of stress and temperature [63,64]. However, although extensive work was performed using this technique for dislocation characterization and properties, analyses are lacking on the nature of dislocations nucleated at scratch sites at room temperature and without subsequent annealing treatment.

Fig. 12 shows the microstructure of a Si sample resulting from a scratch on a $\{0\,0\,1\}$ surface along a $\langle 1\,1\,0\rangle$ direction, with an applied load of 0.45 N [61,65]. No additional stress was applied and no subsequent annealing was performed on that sample. Usually, after annealing, such a scratch orientation is found to produce glide set dislocations mainly on the two $\{1\,1\,1\}$ planes having a common direction perpendicular to the scratch. Thin foils parallel to one of these planes were extracted from the specimen in order to study the deformation microstructure generated by a room temperature scratch. Large perfect glide loops with $1/2\langle 1\,1\,1\rangle$ Burgers vectors were found in the two $\{1\,1\,1\}$ glide planes. They consisted of segments aligned along directions varying between $\langle 1\,1\,2\rangle/30^{\circ}$ and $\langle 1\,2\,3\rangle/41^{\circ}$, plus a few screw segments. When expanding in the glide plane, these loops kept these two low-energy directions, so that the resulting segments with average 60° and 90° orientations exhibited irregular sawtooth shapes. The junctions between

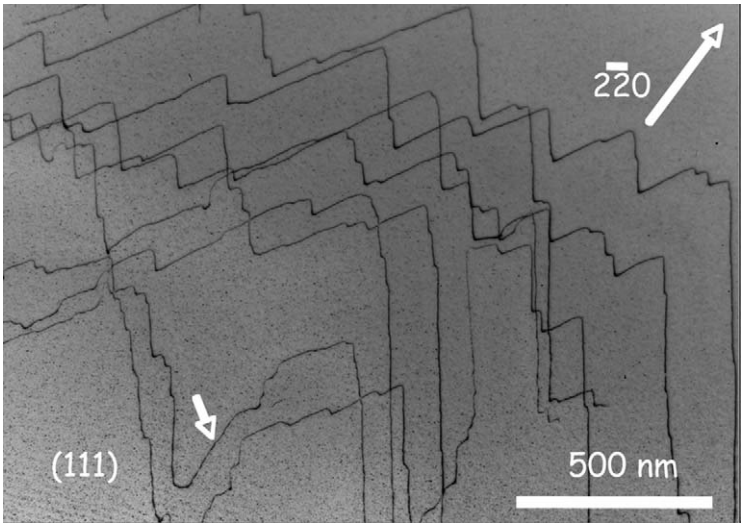

Fig. 12. Microstructure resulting from a scratch at room temperature. Note the roughness of the dislocation lines. Dislocations are aligned along ⟨1 1 2⟩ and ⟨1 2 3⟩ directions. One segment (arrowed) has a screw orientation. After Rabier et al. [65].

two ⟨1 1 2⟩/30° segments located in two Peierls valleys at an angle of 60° acted as strong pinning points.

2.2.4. Deformation substructure in Si indented at low temperature

Asaoka et al. [66] recently revisited the indentation of silicon with the aim of deforming it plastically below room temperature. These authors indented silicon at 77 K and showed that it can be deformed plastically. TEM observations of the microstructure showed dislocations aligned along the ⟨1 1 0⟩ and ⟨1 1 2⟩ directions. Weak-beam dark field showed these dislocations were perfect ones and had $a/2\langle 1\,1\,0\rangle$ Burgers vectors. A HREM observation was also performed on a dislocation seen edge-on, which was shown to have an undissociated core. The exact location of this core, in a glide plane or a shuffle plane, could not be determined.

2.3. What is the transition stress?

Since it appears that two types of dislocations are nucleated in two very different temperature and stress regimes, it is of interest to derive the transition stress at which the nature of the nucleated dislocations change from dissociated to perfect. For that purpose, it is necessary to compare deformation tests performed in very different experimental conditions. In particular, the deformation conditions that produce deformation microstructures containing undissociated dislocations are such

that it is usually difficult to measure the uniaxial yield stress. Thus, two types of stress measurements were performed using TEM and X-ray diffraction.

2.3.1. Stress measurements using TEM

Postmortem TEM characterization of the deformation substructures can be performed after any type of mechanical tests. Such characterizations can be used to determine the stresses experienced by dislocations that were frozen in at the end of a test. In the local line tension approximation and for elastically isotropic materials, the dislocation curvature R under a stress τ can be derived from [67]:

$$\tau = \frac{T(C_{ij}, \alpha)}{bR}, \tag{5}$$

where T is the line tension that depends on the elastic constants C_{ij} and the character α of the dislocation line. Gottschalk [68] showed that this expression could be used in the case of dislocations experiencing high Peierls potentials. In such conditions, the information relevant to the measure of the applied stress is localized in the bends connecting two straight segments that are lying in different Peierls valleys. The curvature radii of these bends are inversely proportional to stress, which makes measurements all the more difficult as the stress is high. This method was applied to different deformation microstructures containing glide dislocations and perfect dislocations. The deformation conditions investigated were chosen in such a way that dislocations were nucleated during mechanical testing without any prestrain. In some tests, the applied stress was measured by usual methods during deformation and a high temperature test was used to check the calculation parameters. For each test several curvature radii were measured and the local stress was estimated using eq. (5). The average curvature radii of dislocations and the resulting stresses are given in Table 1.

From the results given in Table 1, one can see the nature of the observed dislocations is changing for an applied stress value within the interval from 560 to 1100 MPa. Obviously, these data are very scarce and more deformation tests have to be performed to further reduce this stress interval.

Table 1
Stress measurements from curvature radii of dislocations under various deformation conditions of confining pressure (CP) and testing temperature

T, CP	τ (MPa) applied	$\bar{R}$ (nm) measured	$\bar{\tau}$ (MPa) calculated	Nature of dislocations
700 °C, (1)	50	800	×	DG
450 °C, 1.5 GPa (2)	700	75	560	DG
150 °C, 5 GPa (3)	?	40	1100	PD
20 °C, 5 GPa (3)	?	25	1600	PD

Note: DG: dissociated glide dislocation; PD: perfect dislocation. (1) Standard test [55], (2) Griggs apparatus [70], and (3) multi-anvil apparatus [60,61].
Source: After Ref. [69].

2.3.2. Stress measurements using X-ray diffraction

More recently, it became possible to obtain stress–strain curves under pressure in the range of deformation controlled by perfect dislocations and at the transition [71]. This was performed using a deformation apparatus (called D-DIA) that is designed to operate in a synchrotron beamline and allows applying separately the confining pressure and the applied stress [72]. In this experimental setup, the specimen length is monitored by X-ray radiography using platinum foils placed at the specimen ends that are opaque to the X-ray beam. The applied stresses are measured through the shift of X-ray diffraction peaks of polycrystalline alumina rams. Yield stresses were then measured between room temperature and 425 °C under an average strain rate of $2 \times 10^{-5}\,s^{-1}$. Plotting the obtained resolved yield stress versus temperature together with data extracted from several other experimental studies one generates a master curve (Fig. 13), which clearly exhibits an inflection. This inflection is correlated with the occurrence of a deformation controlled by perfect dislocations and occurs at a stress of about 1.5 GPa and a temperature of about 300 °C.

Interestingly, an extrapolation of the yield stresses controlled by dissociated glide dislocations leads to a yield stress $\tau_0 = 15 \pm 5$ GPa $(0.3 \pm 0.1\mu)$ at 0 K [51], whereas an extrapolation of the data obtained in the domain controlled by perfect dislocations yields a flow stress $\tau_0 = 1.5 \pm 0.4$ GPa $(0.03 \pm 0.008\mu)$ at 0 K.

2.3.3. The transition stress

TEM experiments allow one to measure the local stress the dislocations were submitted to when the microstructure was frozen in at the end of the deformation test. Yield stresses can be measured during the tests but, then, they include not only the local stress but also the internal stress. One concludes that perfect dislocations are nucleated at stresses larger than 1.1–1.5 GPa, which corresponds to temperatures

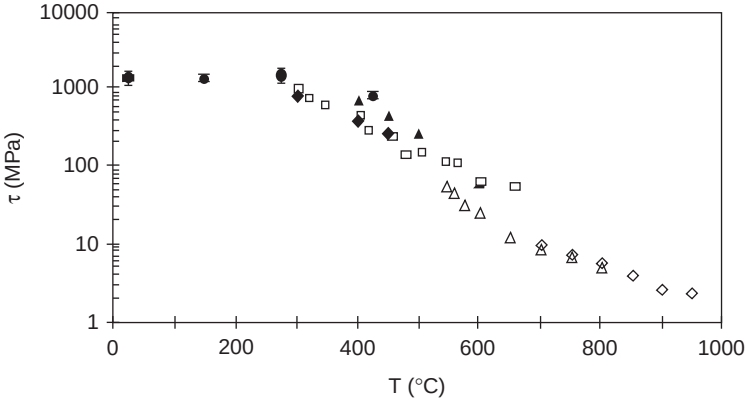

Fig. 13. Logarithm of the resolved yield stress as a function of temperature for Si single crystals, showing a transition around 300 °C. (●) Rabier et al. [71], (♦ and ▲) Castaing et al. [54], (◇ and Δ) Omri [73], and (□) Demenet [55]. After Rabier et al. [71].

lower than 300 °C. An extrapolation of the data of Duesbery and Joós [45] to high stresses predicts that the transition between the deformation mechanisms controlled by dissociated glide dislocations and perfect shuffle dislocations should occur at a stress far lower than the measured ones: about 680 MPa (close to 0.01μ). Such stresses were reached in experiments on virgin materials (see the stress–strain curve at 450 °C in Fig. 7) and dissociated glide dislocations were evidenced. Thus, Duesbery and Joós correctly predicted a change in mechanism at high stresses, but the value of the transition stress should be reconsidered in the light of experimental results.

2.4. The dislocation microstructures at high stress

2.4.1. The signature of low temperature, high-stress deformation

The previous sections clearly show that the low temperature, high-stress deformation microstructures nucleated under resolved shear stresses larger than 1 GPa have particular signatures as compared to usual ones. At the resolution of the weak-beam dark field images, dislocations are found to be perfect ones and they lie in uncommon Peierls valleys like $\langle 1\,1\,2\rangle/30^\circ$ and $\langle 1\,2\,3\rangle/41^\circ$. Strong pinning points are also found along their lines. These features bring evidence of the nucleation of dislocations with different core structures at high stress and low temperature.

The nature of the dislocations not depends only on the applied stress but also on other thermomechanical conditions imposed to the material. Indeed, the same resolved shear stress (about 2 GPa) induces the formation of largely dissociated dislocations when reached after a prestrain ([54]; see Section 2.1.1) and of perfect dislocations when applied to virgin crystals below 400 °C. In these two cases, the dislocations were submitted to stresses larger than the stress for partial decorrelation, since decorrelated partials were observed after a prestrain. This is in agreement with the fact that the perfect dislocations found at high stresses and low temperatures are not glide set dislocations.

2.4.2. The signature of low temperature, high-stress deformation: revisiting previous works

Keeping in mind the striking features of high-stress dislocations, which clearly emerge from the investigations reported above, we reexamine relevant studies published some time ago in a different context.

Hill and Rowcliffe reported dislocations features of the high-stress type after indentation at 300 °C, as can be seen in Fig. 6 of Ref. [53]. These dislocations were not thought to be associated to the deformation process itself; they were assumed to be geometrically required at the ends of block slip displacements of the material under large stresses, close to the theoretical shear stress value. Similar dislocation types were also found by another group after room temperature indentation in the 1970s, but they were assumed to be irrelevant (V.G. Eremenko, private communication).

Most of the high-stress dislocations features can be found in the TEM pictures of published research works on the micromachining of silicon surfaces. Although the mechanism of material removal in the ductile mode must be related to the formation of an amorphous phase, dislocations with average properties looking like those of perfect dislocations were observed in some grinding conditions (see, e.g., [74]). Using cross-sectional TEM, Johansson et al. [75] were also able to image perfect dislocations, besides the presence of cracks, in the vicinity of silicon surfaces polished with 6 μm diamond paste. Their published micrographs show dislocations exhibiting the same original characteristics as those discussed above.

This rapid overview shows that perfect dislocations are systematically present in high-stress dislocation deformation processes. Saka et al. [76] also found out a large dislocation activity resulting from some fatigue process at room temperature. However, the TEM micrographs do not allow one to draw a conclusion about the nature of these dislocations.

2.5. Dislocation core structure and transformation

Since two types of dislocations exist in silicon, namely dissociated and undissociated ones, it is of interest to determine whether they are nucleated in separate temperature and stress domains, or could result from a transformation from one form to the other upon switching from one stress and temperature domain to the other one.

The various authors who observed perfect dislocations assumed that they were located in the shuffle set, as follows from the calculations of Duesbery and Joós [45]. However, there is yet no *direct* experimental evidence about the nature of the plane, glide, or shuffle, in which the core of these perfect dislocations is located.

Several experiments were conducted in order to check the ability of the dislocation cores to undergo transformations. These experiments consist in nucleating dislocations of one type under their specific nucleation conditions and submitting this microstructure to experimental conditions where the other type of core is observed.

2.5.1. From dissociated glide dislocations to perfect dislocations

A specific experiment was designed to check whether dissociated glide dislocations could be transformed into undissociated dislocations [77]. A sample was deformed at room temperature after having been previously deformed in the athermal regime at 1050 °C. It is well known that such a high temperature prestrain leads to a microstructure of weakly dissociated dislocations, mainly of edge character, but that does not contain straight crystallographic segments [78].

The microstructure obtained after room temperature deformation is complex. Nevertheless, several features can be evidenced. In some areas of the thin foil, the microstructure is not different from what is observed in an initially dislocation-free sample. It consists of undissociated dislocations with $a/2\langle 1\,1\,0\rangle$ Burgers vectors elongated along the $\langle 1\,2\,3\rangle$ direction. However, the more frequently observed

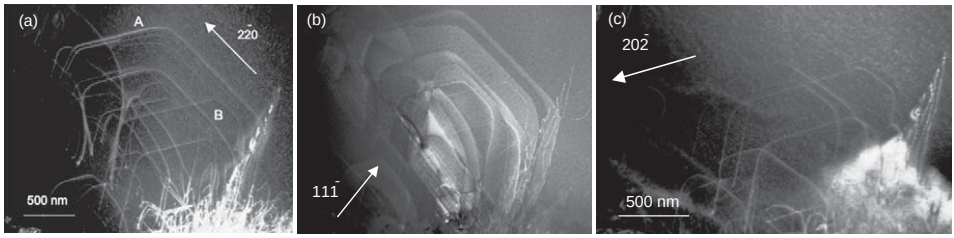

Fig. 14. Dissociated dislocations in the (1 1 1) glide plane of a crystal prestrained at 1050 °C and further deformed at 293 °C under 5 GPa. There are two slip systems, A and B. (a) Weak-beam dark field (2.2g, $g = 2\,\bar{2}\,0$); A and B are in contrast. (b) Weak-beam dark field (7.1g, $g = 1\,\bar{1}\,1$); the stacking fault of A is in contrast, B is in contrast. (c) Weak-beam dark field (3.1g, $g = 2\,0\,\bar{2}$); A is out of contrast, B is in contrast. After Rabier and Demenet [77].

microstructure is made of hexagonal loops of partial dislocations or widely dissociated dislocations. Extra diffraction spots associated to twin bands can also be evidenced in some areas. Examples of hexagonal dislocation loops are shown in Fig. 14. Two glide systems A and B are associated to these loops, which are lying in {1 1 1} planes and are composed of $\langle 1\,1\,0 \rangle$ segments. Contrast analysis (Fig. 14) shows that slip system A contains only one type of partial dislocations, with Burgers vector $a/6[1\,\bar{2}\,1]$. These partial dislocations arise from the dissociation of dislocations with $a/2[1\,\bar{1}\,0]$ Burgers vector into $a/6[1\,\bar{2}\,1] + a/6[2\,\bar{1}\,\bar{1}]$. The dislocations found in slip system B have a Burgers vector $a/2[0\,\bar{1}\,1]$ and are dissociated into $a/6[1\,\bar{2}\,1] + a/6[\bar{1}\,\bar{1}\,2]$. Hence, there is a large difference in splitting widths between the two systems.

Clearly, the hexagonal loops, widely dissociated half-loops, and twin bands are related to dislocations created during the high temperature prestrain. From their initial dissociated configurations, these dislocations moved under the high stress applied at room temperature and were blocked into $\langle 1\,1\,0 \rangle$ Peierls valleys. The latter are the signature of dissociated dislocations of the glide set [2,14]. Furthermore, the application of a high stress can lead to the motion of uncorrelated partials, partial dislocation sources as well as to twinning. These results show that it is also difficult to transform dissociated glide dislocations into perfect dislocations. In short, at room temperature and under high stress, mobile dislocations of the glide set have the same $\langle 1\,1\,0 \rangle$ Peierls valleys as at high temperature and remain dissociated.

2.5.2. *From perfect dislocations to dissociated glide dislocations*

Rabier and Demenet [69] performed *in situ* annealing in a transmission electron microscope in order to promote the transformation of perfect dislocations into dissociated glide dislocations. A low-deformation microstructure was obtained at room temperature and under a pressure of 5 GPa in the conditions described in Section 2.2.1. It contained perfect dislocations with their usual character, like $\langle 1\,1\,2 \rangle/30°$, as well as cracks. This sample was annealed in the heating stage of a

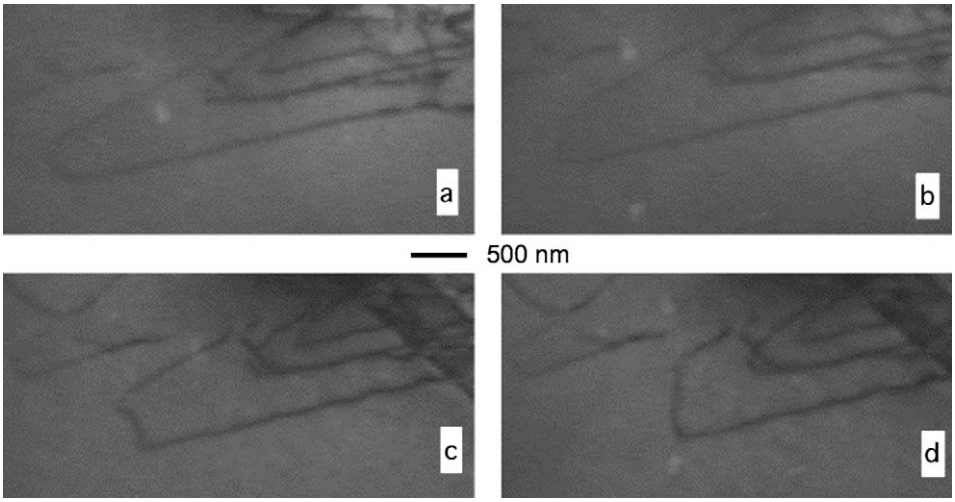

Fig. 15. Snapshots taken during an *in situ* anneal of undissociated dislocations up to 685 °C in the TEM. After Rabier and Demenet [69].

JEOL 200CX electron microscope at temperatures up to 685 °C. The evolution of the microstructure was recorded with a video camera.

Fig. 15 shows snapshots of a recording that was taken during an annealing time of 90 min. Evidently, there is no major evolution in the shape of the perfect dislocation glide loops. Only the front of the loops moves, dislocation segments staying locked in the $\langle 1\,1\,2\rangle/30^\circ$ and screw Peierls valleys. This shape evolution provides no evidence of a transformation. However, in an area of the same thin foil that initially looked free of dislocations (but not of cracks), the annealing treatment induced the nucleation at crack edges of glide loops with hexagonal shapes characteristic of the glide set dislocations (Fig. 16).

This experiment reveals no evidence of a massive transformation of preexisting perfect dislocations. It rather shows nucleation events of glide dislocations from lateral crack surfaces, where undissociated dislocations are nucleated at room temperature and under high stresses.

Asaoka et al. [66] also performed TEM *in situ* annealing on thin foils cut from indented samples at 77 K. Annealing the microstructure of perfect dislocations at 673 K produced no change in the dislocation configurations. At 973 K, different dislocation configurations were evidenced, in which dislocations were dissociated and the lines were either curved or lying along $\langle 1\,1\,0\rangle$ directions. These dislocations of the glide set were connected to perfect dislocations that were assumed to be shuffle dislocations. In parallel, the initial microstructure of shuffle dislocations was not significantly modified. The authors concluded that shuffle dislocations are still immobile at 973 K.

Saka et al. [76] used a FIB-machined sample designed in such a way as to be saturated with interstitials, in order to study the possible shuffle to glide

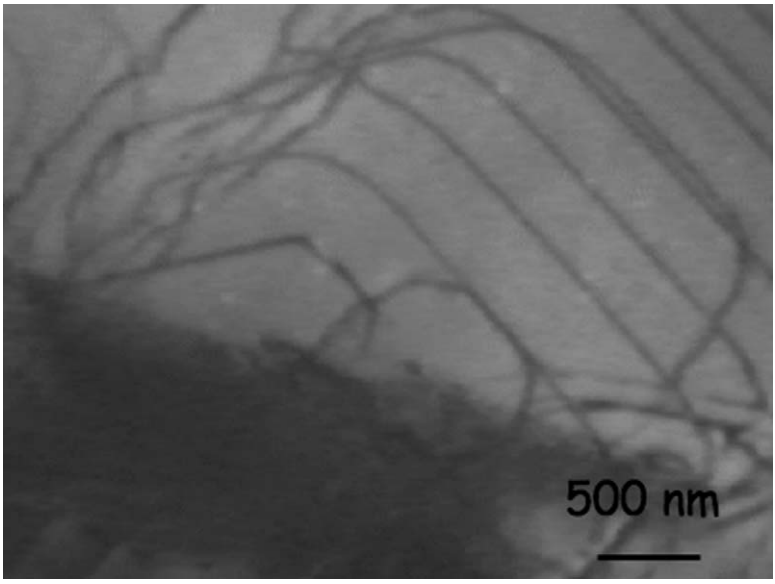

Fig. 16. Nucleation of dislocations having the signature of glide set dislocations from lateral surfaces of cracks during *in situ* annealing. After Rabier and Demenet [69].

transformation in the presence of point defects. A transformation started after annealing at around 400 °C and seemed to be initiated at, or at least near, sharp bends of the preexisting shuffle set dislocations. In the place of perfect dislocations, which had moved away, faint contrast effects were found that were attributed to debris or dislocation loops.

Hill and Rowcliffe [53] have annealed *in situ* a sample indented at room temperature and found analogous features. The effect of annealing could be distinguished after 30 min at 550 °C, but became substantial only after 1 h at 600 °C. These annealing experiments show that 30° dislocations do not move at high temperature under the residual stress present in indented samples. Rather, bowed-out non-screw segments are seen to move rapidly, trailing long screw segments.

2.5.3. Conclusions about the evidences of dislocation core transformations

These experiments, which were aimed at changing the nature of the core structure of dislocations, provide the following evidence:

- Dissociated glide dislocations do not transform into perfect dislocations at low temperature and high stress. The dissociation widths increase under the application of a high stress, which prevents the occurrence of any transformation. In the case where the applied stress induces a narrowing of the splitting width, Demenet [55] and Grosbras et al. [79] demonstrated that it is impossible to recombine a dissociated configuration.

- Perfect dislocations resulting from high-stress deformation do not move significantly in the temperature range where glide dislocation usually nucleate.
- There is no massive transformation of perfect dislocations. Rather, some nucleation events occur, from which glide dislocation can move away and multiply contribute to relax the initial microstructure. In these experiments, no external stress was applied: the driving forces were either the residual mechanical stresses resulting from the previous treatments or the chemical forces built up from a supersaturation of interstitials.

2.6. Physical signatures associated to perfect dislocations

More insight about the actual core structure of perfect dislocations can be obtained from their influence on the physical properties of the material. For these reasons, physical characterizations of samples deformed at high stress and low temperature were performed.

Experiments were designed to compare by means of positron annihilation the defect populations after plastic deformation at high and low temperatures, which are expected to contain different populations of point defects [80]. After room temperature deformation, rather stable vacancy clusters appear and no evidence is found for positron capture by dislocations. In contrast, after high-temperature deformation (800 °C), positrons are trapped in large vacancy clusters and dislocations acting as combined traps. These point defects signatures show clearly that the deformation mechanisms depend on temperature and stress. However, the way the different dislocation structures formed during high-stress deformation at room temperature influence point defect generation is an open question.

The physical properties of perfect dislocations, which are assumed to be shuffle ones, were mainly probed through photoluminescence (PL) measurements. Pizzini et al. [81] performed PL measurements on samples that were deformed following the procedures reported in Section 2.2.1.

Typical PL spectra of samples deformed at room temperature and 150 °C are shown in Fig. 17. They are rather different from those typical of glide dislocations. The canonical emission related to glide dislocations, which consists of a quartet of lines conventionally labeled D1–D4, at about 0.807, 0.877, 0.945, and 1.00 eV [82], is in fact absent. The PL spectrum of the sample deformed at room temperature presents instead a broad emission at about 0.8–0.9 eV, whose shape is influenced by the detector cutoff, and three narrow peaks at 0.973, 1.003, and 1.023 eV that emerge from the background.

In the sample deformed at 150 °C [Fig. 17(b)], the narrow peak intensities are strongly reduced and an additional contribution to the background is observed around the Si free-exciton emission at 1.1 eV. In addition, an asymmetric and broad emission peaked at 1.029 eV is replacing the sharp peak at 1.023 eV that is observed in the sample deformed at room temperature [Fig. 17(a)]. It was suggested that the peak at 1.029 eV is the superimposition of two different spectral contributions.

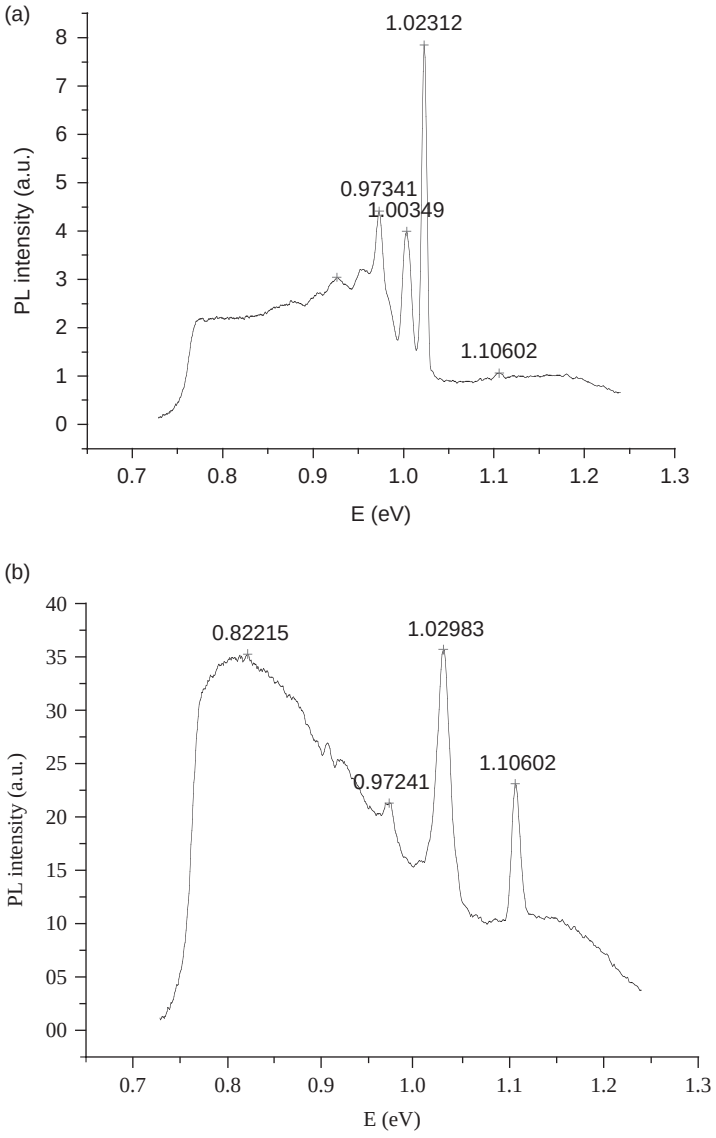

Fig. 17. Photoluminescence spectra of deformed silicon. (a) At room temperature, under 5 GPa and (b) at 150 °C, under 5 GPa. After Pizzini et al. [81]. See text for detail.

Since the PL spectra do not show any evidence of specific emissions associated to shuffle dislocations, Pizzini et al. [81] concluded that perfect dislocations present a reconstructed core, and their generation is accompanied by the introduction of point defects and point defect clusters. A broad band around 1 eV is the only PL

feature that could be directly related to perfect dislocations; it was explained by the conjecture that gap changes are induced by the dislocation strain fields.

Steinman et al. [83] used samples analogous to those investigated in Ref. [81]. The samples were subjected to isochronous anneals at and above 300 °C. Fig. 18 shows PL spectra of the sample after deformation at room temperature under a hydrostatic pressure of 5 GPa and a subsequent anneal at 300 and 400 °C. After annealing at 300 °C, the PL intensity increases significantly. This can be interpreted as unresolved dislocation-related luminescence (DRL) due to the presence of typical features at D1–D4 line positions. In parallel, the intensity of the band exhibiting a maximum at 1.02 eV rapidly decreases. Further annealing at 400 °C leads to an increase of DRL and a significative increase in the resolution of D4 and D3 bands. As these bands are usually attributed to straight segments of dissociated 60° dislocations, this change in DRL after annealing of a microstructure of perfect dislocations is consistent with the PL signature attributed to dissociated dislocations of the glide set.

These PL experiments indicate some trends about the atomic structure of the perfect dislocations:

- They are likely to be reconstructed.
- Their signatures are convoluted with that of point defects.

As far as core modifications or nucleation of glide dislocation are concerned, it appears that a transition in the signature of PL spectra after annealing gives a

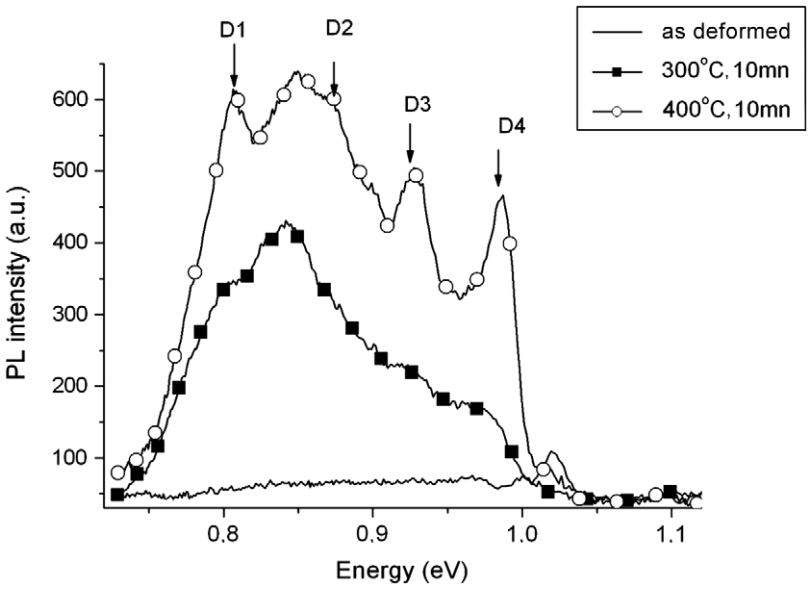

Fig. 18. Photoluminescence spectra of deformed silicon: annealing effects. See text for detail. After Steinman et al. [83].

transition temperature lower than the one found by *in situ* TEM annealing. Two explanations can be put forward for explaining this discrepancy. TEM is able to show up local events with no statistical significance, whereas PL spectra are sensitive to modifications in the bulk material or to premonitory mechanisms associated to the nucleation of glide dislocations. In addition, the PL signatures attributed to perfect dislocations disappear as soon as the transformation occurs, which is not consistent with TEM observations. This could be explained by some modifications in the signatures of perfect dislocations as a function of temperature (see Ref. [81]).

3. The core structure and mobility of perfect dislocations

Understanding the plastic properties and the nucleation of dislocations at high stress requires knowledge of the actual core structure of perfect dislocations. The major problem is to determine the location of those perfect dislocations, that is, whether they are lying in a shuffle plane or a glide plane. Although one expects perfect shuffle dislocations to be found at high stress, from an extrapolation of the calculations by Duesbery and Joós [45], the apparent agreement of experiments with these calculations needs to be confirmed. However, establishing unambiguously the shuffle or glide nature of dislocations proved to be very difficult even for the ''usual'' dislocations. This fed in the past the debate on the actual core structure of dislocations in silicon. The straightforward method for core structure determination is high-resolution electron microscopy (HREM). For usual dislocations, it was necessary to resolve the $\langle 1\,1\,0\rangle$ dumbbells for a dislocation aligned along $\langle 1\,1\,0\rangle$ Peierls valleys, that is, to discriminate between two atoms 0.14 nm apart in the crystal projection. Although corrected HREM can nowadays achieve this resolution quite routinely on perfect crystals, the actual structure of dissociated dislocations in silicon has not been revisited and this problem is still open. The same kind of HREM needs to be carried out on undissociated $\langle 1\,1\,2\rangle/30^\circ$ dislocations, which control the high-stress, low-temperature plastic deformation of silicon. The challenge appears to be far more difficult since $\langle 1\,1\,2\rangle$ dumbbells need to be resolved, which are composed of two atoms 0.078 nm apart in projection. Recently, such a resolution was achieved on a perfect silicon crystal using a corrected STEM [84], but high-stress dislocated crystals have not yet been investigated by this technique. In this context, and as was previously done for dissociated glide dislocations, only indirect methods are available to check whether those perfect dislocations are in the shuffle set or not.

Analyzing the core geometry is a first step that can also provide useful information on the low-energy configuration of perfect dislocations. Indeed, this was already performed long ago by Hornstra [10], but these results have to be revisited in view of the new data obtained on high-stress microstructures. Furthermore, most of the work done since the advent of the weak-beam technique (see Section 1) has focused on dissociated dislocations in the glide set.

In addition, atomistic studies were performed to calculate how stable core configurations and Peierls stresses of perfect dislocations depend on the atomic

location of the core. Such calculations were also performed to study the nucleation of dislocations from a surface step. Atomistic calculations of dislocation cores in silicon, using interatomic potentials and *ab initio* methods, benefited from most of the simulation techniques available to date. Long-range deformation fields associated to dislocations were tackled using either periodic or cluster-like conditions.

Not only were calculations done for looking at the structural properties of straight dislocations, but elementary kinks of atomic dimension were also investigated. Peierls stresses were determined either by applying a stress on the dislocation core or by using methods like the nudged elastic band (NEB), which are useful for determining transition configurations and energies. These techniques and their limitations are discussed in several papers (see, e.g., [32,85]).

3.1. General features of perfect dislocations in the shuffle plane: a geometrical analysis

The lowest energy partials of the glide type contain lines of atoms with dangling bonds lying almost in the {1 1 1} glide plane and allowing for easy reconstruction. In contrast, shuffle dislocations – besides screw dislocations that are discussed in Section 3.2.1.1 – exhibit dangling bonds, which are parallel and normal to the glide plane. This geometry is *a priori* unfavorable for the pairing of bonds. This is the reason why it is of interest to check the density of dangling bonds along dislocations as a function of their line orientation in the shuffle plane. Hornstra was the first to perform this analysis [10]; he found out that the density of dangling bonds increases from $\langle 1\,1\,2\rangle/30^\circ$ to $\langle 1\,1\,0\rangle/60^\circ$ and $\langle 1\,1\,2\rangle/90^\circ$ for perfect dislocations with 1/2 $\langle 1\,1\,0\rangle$ Burgers vector. This simple analysis is in good agreement with the observation of high-stress microstructures built with $\langle 1\,1\,2\rangle/30^\circ$ perfect dislocations.

However, the variability of dislocation orientations found in experiments between $\langle 1\,1\,2\rangle/30^\circ$ and $\langle 1\,2\,3\rangle/41^\circ$ lines has prompted one of us to consider the geometry of kinks on $\langle 1\,1\,2\rangle/30^\circ$ and the ability for reconstruction of dangling bonds in the dislocation cores [86]. Since the dangling bond density on the $\langle 1\,1\,2\rangle/30^\circ$ dislocation is low, the dangling bonds are far apart and their reconstruction is unlikely. Then, in order to overcome the conflict between a low dangling bond density and reconstruction, such reconstructions could occur on $\langle 1\,1\,2\rangle/30^\circ$ dislocations showing geometrical kinks. Indeed, a dislocation built with $\langle 1\,1\,2\rangle/30^\circ$ and $\langle 1\,1\,0\rangle/60^\circ$ segments can achieve both a dislocation line with a low dangling bond density and the possibility for those dangling bonds to reconstruct. Then a stable $\langle 1\,2\,3\rangle/41^\circ$ segment is obtained, consistent with the observation of such a Peierls valley at high stress (see Fig. 19). Furthermore, the lattice distortions associated with such a reconstruction could be minimized at kink sites.

Such dangling bond geometry appears on {1 1 1} cleaved surfaces, which exhibit a (2×1) reconstruction as was proposed by Pandey [87]. In this surface reconstruction, dangling bonds attach to in nearest neighbors and share π bonding. This

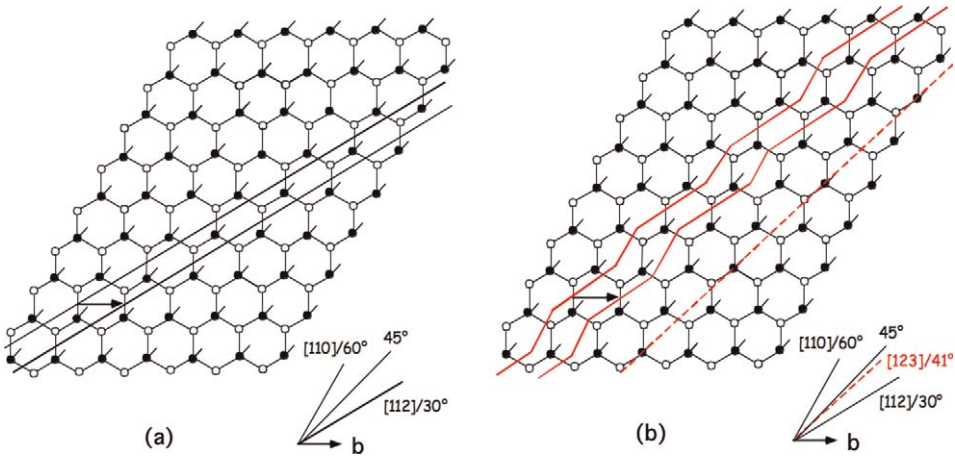

Fig. 19. (1 1 1) glide plane viewed in the shuffle set and showing dangling bonds. The edge of the supplementary plane of a dislocation is indicated. (a) $\langle 1\,1\,2\rangle/30^\circ$ dislocation and (b) $\langle 1\,1\,2\rangle/30^\circ$ dislocation with $\langle 1\,1\,0\rangle$ kinks; this allows for bond pairing and results in a $\langle 1\,2\,3\rangle/41^\circ$ dislocation. After Rabier [86].

surface reconstruction is metastable and is irreversibly transformed into the (7×7) stable configuration by annealing at 600 °C. Such a (2×1) reconstruction was also recently found in *ab initio* calculations [88] during the propagation of a crack in silicon. A reconstruction of this type is exemplified in the case of a $\langle 1\,1\,0\rangle/60^\circ$ dislocation segment located at a kink site in which dangling bonds were put in nearest neighbor positions, as in the case of {1 1 1} surfaces (see Fig. 20). Then a π bond can be formed; this is accompanied by a deformation of the lattice perpendicular to the dislocation line. If such a configuration could be obtained in the case of the $\langle 1\,1\,0\rangle/60^\circ$ dislocation, other line directions would not favor dangling bonds in nearest neighboring positions. However, the strained and "dangling" bonds present in the core of unreconstructed segments could permit the trapping of impurities and intrinsic defects, which may be relevant to the observation of strong pinning points.

3.2. Atomistic calculations

Atomistic computations were performed for 60° and screw dislocations, which are of interest since perfect dislocations of this type appear to be very mobile and are likely to be important in the glide loops development and location. $\langle 1\,1\,2\rangle/30^\circ$ and $\langle 1\,2\,3\rangle/41^\circ$ dislocations were not investigated yet, mainly because calculations are difficult owing to the low periodicity along the dislocation lines.

3.2.1. Perfect dislocation structure and stability

3.2.1.1. Screw dislocations. It is often assumed that screw dislocations govern the plastic behavior in materials with high Peierls stresses, because of their usually low

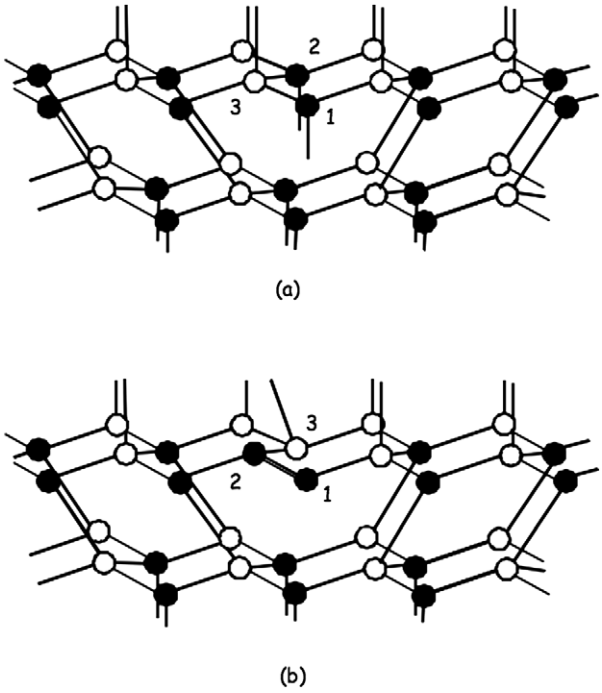

Fig. 20. Possible reconstruction at kinks. (a) Perfect 60° shuffle dislocation with dangling bonds in 1 and 2. (b) Perfect 60° shuffle with a π bond. Dangling bonds have been exchanged between 2 and 3 positions, and pairing of bonds has occurred between 2 and 1. This reconstruction is expected to be feasible at kink sites. After Rabier [86].

mobility related to their ability to dissociate in a sessile way. Their ability to cross slip can also favor a change in core location, for example, between glide and shuffle sets. This explains why several previous investigations were devoted to the structure and stability of the screw dislocation core. From the analysis of the diamond-cubic structure, Hornstra first proposed two possible core structures for the undissociated screw dislocation, located either in a shuffle plane or in a glide plane [10]. The shuffle core was relaxed using first-principles calculations by Arias and Joannopoulos [89]. Another study based on first-principles calculations confirmed that a shuffle core was energetically favored [90]. However, more recently, it was suggested that a glide core reconstructed along the dislocation line is the most stable configuration [91]. Finally, we mention that a new configuration, with a mixed shuffle–glide core at the intersection of the glide and shuffle sets, was proposed by Koizumi et al. on the basis of interatomic potential calculations [92]. Fig. 21 shows all these possible core structures.

The shuffle configuration (A) is characterized by the conservation of the original coordination for atoms in the vicinity of the core, though at the expense of strong bond distortions. For instance, bonds close to the core and linking atoms on both

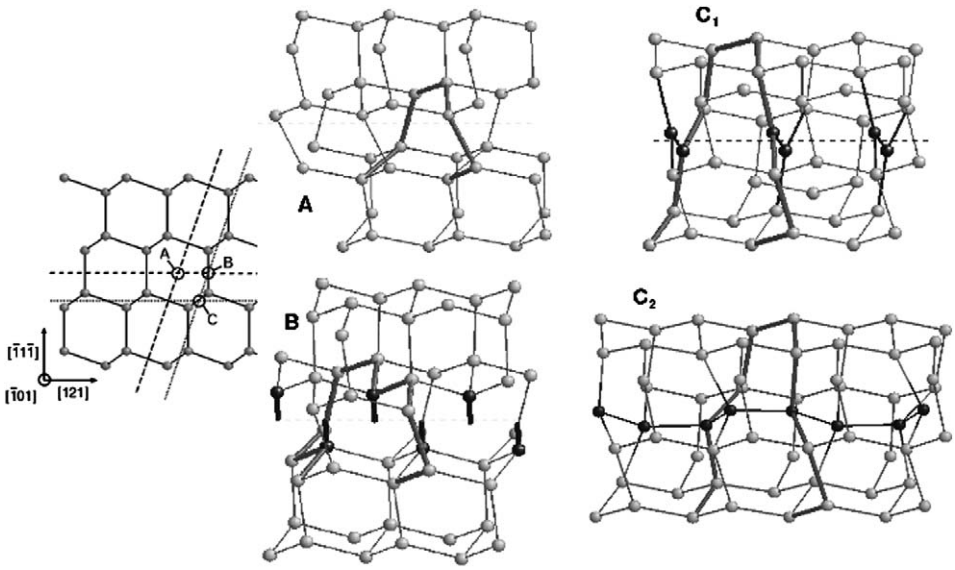

Fig. 21. Possible core configurations for a non-dissociated screw dislocation: shuffle (A), mixed shuffle/glide (B), simple period glide (C_1), and double-period glide (C_2). Thicker dark gray bonds show a Burgers circuit; the dislocation line along $\langle 1\,1\,0 \rangle$ is marked by a dashed line in each case. Atoms located in the immediate vicinity of the core are represented by black spheres. After Pizzagalli et al. [90]. The A, B, C positions for a screw dislocation are shown in the insert on the left side of the figure.

sides of shuffle planes are disoriented by about 20° compared to the bulk [89,90]. The mixed shuffle–glide core (B) involves the breaking of bonds along the dislocation line, apparently resulting in a double row of dangling bonds. As already remarked by Hornstra, such a configuration is likely to be unstable due to symmetry considerations [10]. The simple period glide configuration (C_1) corresponds to a core composed of 3-coordinated atoms, with coplanar bonds and bond–bond angles of approximately 120°, pointing to sp^2 hybridized states. The computed distance between two 3-coordinated atoms is 0.216 nm, to be compared with 0.235 nm, the bulk nearest neighbor distance [93]. Finally, the double-period glide configuration (C_2) allows recovery to a core with only 4-coordinated atoms, after some atomic rearrangements starting from the C_1 glide configuration. The dislocation core is made up of two $\langle 1\,1\,0 \rangle$ rows of dimers, with a dimer length of 0.247 nm, both rows being connected by bonds having a length equal to 0.237 nm.

The relative stabilities of the possible core configurations obtained with different computational methods are reported in Table 2. All performed calculations suggest that the most stable core for a non-dissociated screw dislocation is located in the glide set, with a double period along the dislocation line. The shuffle core A is the second best solution. Electronic structure calculations all indicate that the B core is

Table 2
Relative stabilities of possible core configurations for a non-dissociated screw dislocation (in eV/Burgers vector), computed with different methods

Screw core	Methods						
	Stillinger–Weber potential	Tersoff potential	EDIP	Tight binding DFTB [94]	First principles [91]	Tight binding [91]	First principles [90]
A	0.19	0.31	0.07	0.60	0.54	0.62	0
B	0.05	1.39	0.30	×	×	×	0.32
C_1	1.81	0.85	0.81	×	×	×	0.86
C_2	0	0	0	0	0	0	×

Note: For each column, the zero energy reference is the lowest energy configuration. × means that the value is not available or the considered configuration was found unstable.

unstable, as originally predicted [10]. This casts some doubts on the validity of classical potentials results, especially Stillinger–Weber, for which B is the second best solution, very close to C_2.

Obviously, it is difficult to explain these results by considering the relaxed core structures. Originally, the shuffle core A was thought of as the best option, since the dislocation center is as far as possible from lattice atoms, thus minimizing the deformation. Nevertheless, the reconstruction leading to the glide configuration C_2 apparently allows obtaining a narrow dislocation core with weaker bond distortions.

3.2.1.2. 60° dislocations. The other non-dissociated dislocation that is apparently found to be very mobile during plastic deformation of zinc-blende materials is the 60° dislocation. In his seminal work, Hornstra proposed a possible structure for the 60° dislocation with a core centered in a shuffle plane [10]. This configuration named S_1 here and represented in Fig. 22 has the particularity to include a 3-coordinated atom, with a dangling bond oriented along a $\langle 1\,1\,1 \rangle$ direction. This dislocation core appears to have a high mobility compared to the screw dislocation; it was identified in previous theoretical works with either classical potentials or *ab initio* calculations [95–97]. Nevertheless, the situation is maybe more complex since other possible configurations are stable with a lower core energy. In Fig. 22, we show two of those, obtained from interatomic potential or tight-binding calculations. The glide core G has a very low energy, making it the most stable. The other shuffle core, named S_2, is less stable than the glide core, but still with a lower energy than S_1.

3.2.2. Dislocation mobility

3.2.2.1. Perfect screw dislocation: Peierls stress and energy. There were several early attempts to calculate the Peierls stress of the non-dissociated screw dislocation in silicon [92,98,99]. Empirical potential computations give values ranging from

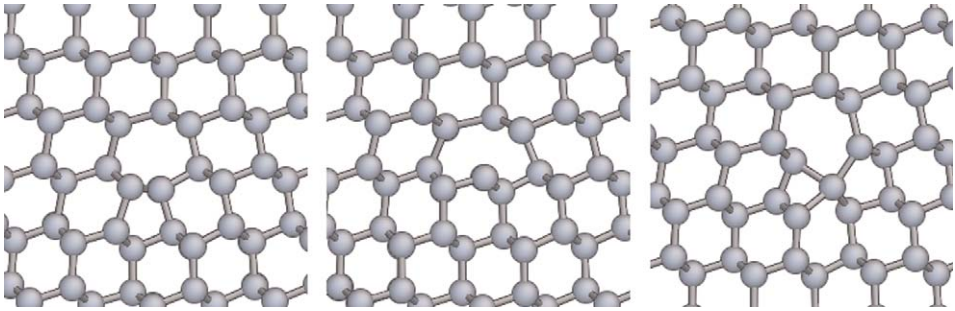

Fig. 22. Three possible core configurations for a non-dissociated 60° dislocation: one glide G (left) and two shuffle, S_1 (middle) and S_2 (right).

0.013 to 0.048 eV/Å^3 (0.03μ to 0.11μ). This large range highlights the difficulty in obtaining accurate values from interatomic potentials in the case of silicon and points at the necessity of using first-principles methods. However, as shown previously, the latter only can be employed in association with small computational systems, for which a careful treatment of boundaries is required. This problem is even more crucial for Peierls stress determination since approaches developed to take boundaries into account are not well suited for treating the displacement of dislocations.

In fact, applying an increasing stress progressively shifts the dislocation, therefore modifying the surface–dislocation interaction in the case of a cluster calculation, or the dislocation–dislocation interaction in the case of periodic boundary conditions. These undesirable effects have to be accounted for if one aims to obtain an accurate value of the Peierls stress in small systems.

This issue has been tackled in the case of the shuffle screw dislocation in silicon [100]. The computed Peierls stress, corrected for spurious boundary interactions, is equal to 0.026 eV/Å^3 or 0.07μ. This value is much lower than measured Peierls stresses for partial dislocations [101]; it can be compared to the Peierls stress of the glide core C_2, which has also been recently computed with a value of about 0.04 eV/Å^3, that is, 0.11μ [91]. The glide configuration appears more difficult to displace under applied stress than the shuffle configuration, possibly because of the presence of reconstructed bonds in its core.

Besides the Peierls stress, a related and interesting quantity for characterizing the mobility of dislocations is the Peierls energy, which is simply the energy barrier to overcome for displacing a straight, infinite dislocation in the lattice. This energy is difficult to compute using standard relaxation techniques, since it is necessarily associated with an unstable dislocation structure. Attempts to extract the relevant information from molecular dynamics simulations have been made [102]. However, the proposed method is tricky and appears more suited for interatomic potentials than for first-principles calculations. Recently, it was proposed to combine both the nudged elastic band method [103] and first-principles calculations performed with periodic boundary conditions, in a way that allows to determine the energy and structure of a dislocation for any migration path [85]. In the case of the non-dissociated screw in

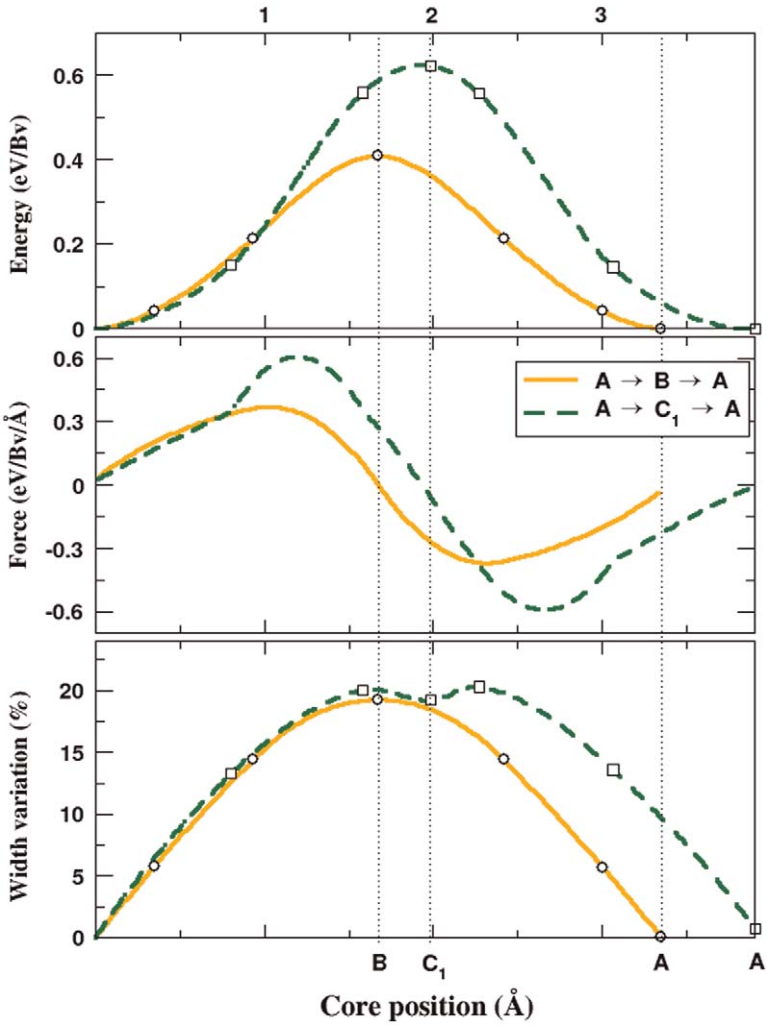

Fig. 23. Variation of dislocation energy (top), its first derivative, that is, the force exerted on the dislocation by the lattice (middle), and dislocation core width (bottom) as a function of the position of a non-dissociated shuffle screw dislocation. The calculations are performed along two possible paths that are indicated in the middle figure. After Pizzagalli et al. [85].

silicon, the computed energy variation as a function of the dislocation position along two possible paths is shown in Fig. 23. The one with the lowest Peierls energy corresponds to the displacement direction previously obtained from calculations using an imposed shear strain [100,104]. The derivative of the calculated energy variation as a function of the dislocation position is the force on the dislocation due to the lattice (Fig. 23). The maximum along the path corresponds to the maximum resistance of the lattice to the dislocation displacement. Converting this force into stress is

straightforward and leads to a value of about $0.025\,eV/Å^3$, in close agreement with previous Peierls stress determinations [100]. Although the computational cost is high due to the use of NEB, there is no need to use boundary corrections with this technique. Another advantage is the possibility to explore high-energy directions for displacing dislocations such as $A \rightarrow C_1 \rightarrow A$, which are not accessible when using imposed shear strain calculations [100].

Finally, information on the structure of a dislocation can be gained from combined NEB and first-principles calculations. For instance, the displacements of core atoms leading to the dislocation migration can be monitored. In the case of the shuffle screw dislocation, the variation of the core width during the displacement was investigated and is represented in Fig. 23. Clearly, the dislocation core expands when the dislocation is centered in an unstable configuration. A possible explanation is that the system gains energy by spreading out atomic displacements, thus minimizing deformation in the dislocation center. Investigations of higher moments of the displacements distribution should provide additional information on the dislocation geometry, such as core asymmetry.

3.2.2.2. Perfect screw dislocation: mobility by formation and migration of kinks. Partial dislocations are known to move at high temperature by the formation and migration of kink pairs, both being thermally activated processes [12]. Non-dissociated perfect dislocations are obtained at lower temperatures and for higher stresses, but since the lattice resistance to dislocation motion is large in silicon, thermal activation is also expected to play a nonnegligible role in that case. Nevertheless, there were very few theoretical studies of kinks on perfect dislocations and those exclusively concern the screw dislocation. Hence, Koizumi and Suzuki investigated the kink velocity as a function of the applied stress and the energy dissipated during kink motion [105]. Their use of a high-energy core configuration does not allow extracting quantitative data regarding the energetics and structure of a single kink.

Recently, Pizzagalli et al. used both interatomic potentials (EDIP, Lenosky) and first-principles methods to study the formation and migration of a kink pair on a perfect shuffle screw dislocation [106,107]. Dislocations and kinks were modeled using silicon clusters (large for potentials, small and passivated with hydrogen atoms for first-principles calculations), one or two kinks being included in the simulation system (Fig. 24). In this work, an unbiased and exhaustive search for all possible configurations of a kink was made initially thanks to the dimer method [108]. This method is particularly useful for studying structural defects with complex reconstructed cores, for which many nonintuitive configurations may exist such as, kinks on partial dislocations in silicon [33]. Thereafter, the migration and formation mechanisms were determined using the nudged elastic band technique. Interestingly, few stable kink configurations were obtained, in contrast with the situation prevailing for partials [33]. This might be explained by the fact that the core of the shuffle screw dislocation is not reconstructed.

Fig. 25 shows two possible structures of a kink. Both are degenerate in energy, at least at the level of the accuracy of first-principles calculations. The first one, called

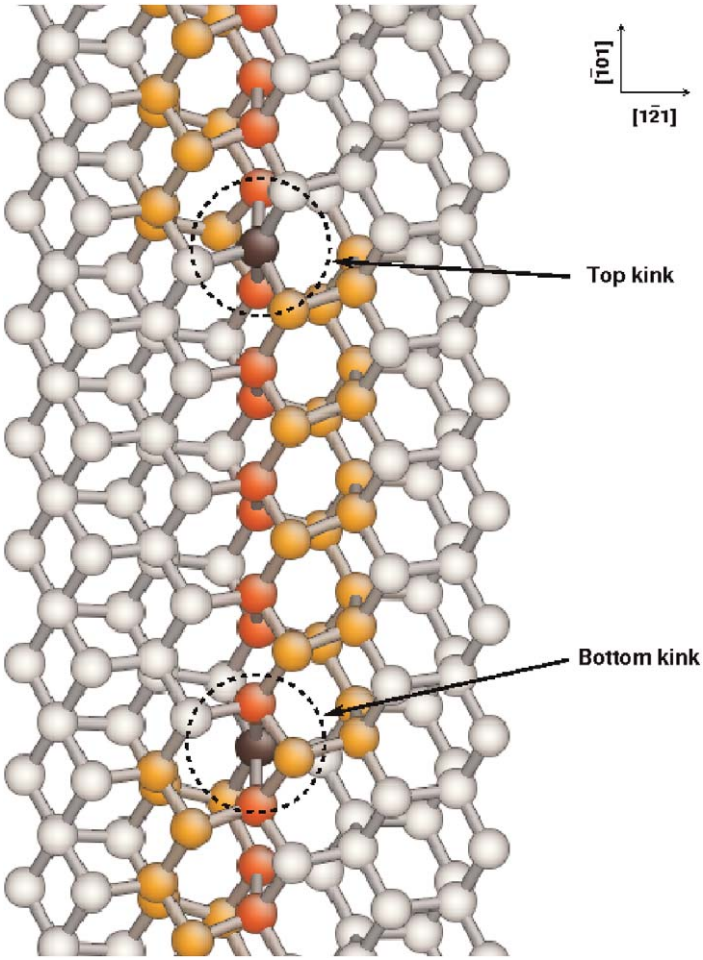

Fig. 24. Ball and stick representation of kinks on a non-dissociated shuffle screw dislocation. Gray atoms indicate screw core atoms while kinks are marked by black atoms. After Pizzagalli et al. [106].

the narrow kink in Ref. [106], is characterized by a 5-coordinated atom in its center, whereas in the second one, called the dangling bond (DB) kink, the central atom is 3-coordinated. Both cores have in common distorted and stretched bonds, with a bond length increasing by 7–13% and an angular deviation greater than 30°. Following a procedure that allows one to obtain the energetics of a single kink in small clusters, the single kink formation energy F_k was determined to be 1.36 eV. With interatomic potentials and EDIP, the narrow kink structure is found to favored. Instead, the Lenosky potential gives the DB kink structure as the most stable configuration. The formation energy of a single kink computed with EDIP is $F_k = 0.91$ eV.

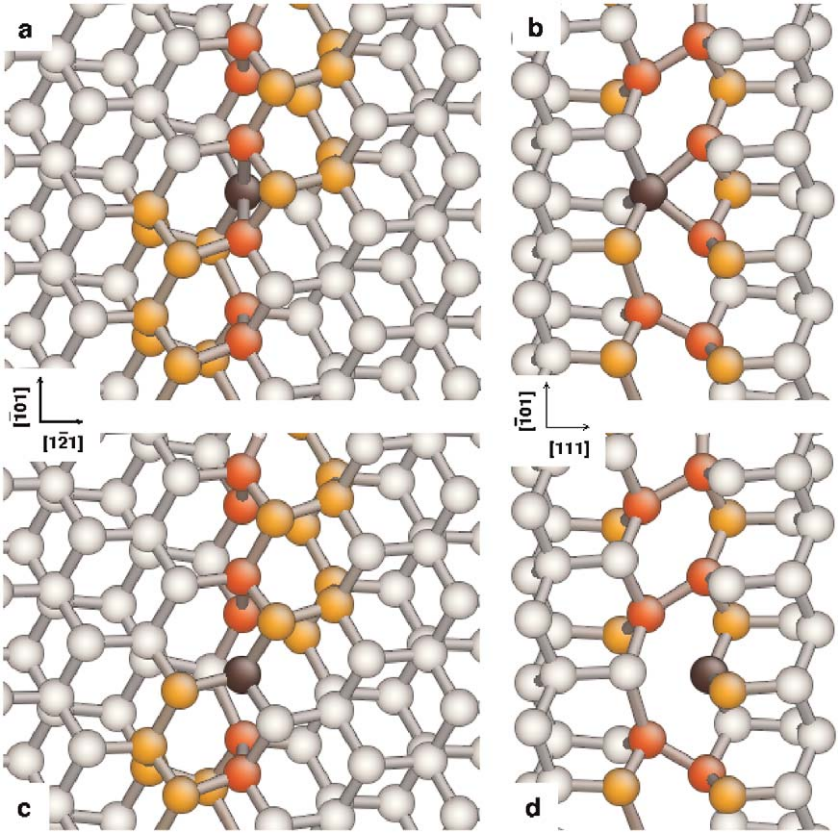

Fig. 25. Ball and stick representations of two possible kink structures shown along two different orientations (left and right). (a and b) Narrow kink and (c and d) DB kink. After Pizzagalli et al. [106].

Nudged elastic band and dimer calculations were also carried out by the same authors in order to investigate the migration of a kink along the shuffle screw dislocation line [106,107]. Fig. 26 shows the migration mechanism corresponding to the displacement of a single DB kink separating from a symmetric kink, using first-principles calculations. Migration of the kink requires first the formation of a bond between the 3-coordinated atom and one of its neighbors, which then becomes 5-coordinated. This configuration is the narrow kink. After the breaking of one bond, the structure recovers the original DB kink configuration, shifted by a Burgers vector b along the dislocation line. Because bonds in the center of the kinks are largely distorted and stretched, the energy variations for forming and breaking bonds are small, yielding a low kink migration energy. Extrapolating values for an infinite kink–kink separation, the first-principles kink migration energy W_m is estimated to be lower than 50 meV. The kink migration mechanism determined with the Lenosky potential is similar, with almost identical migration energy [107]. With EDIP, a slightly different process is obtained since the initial state is the

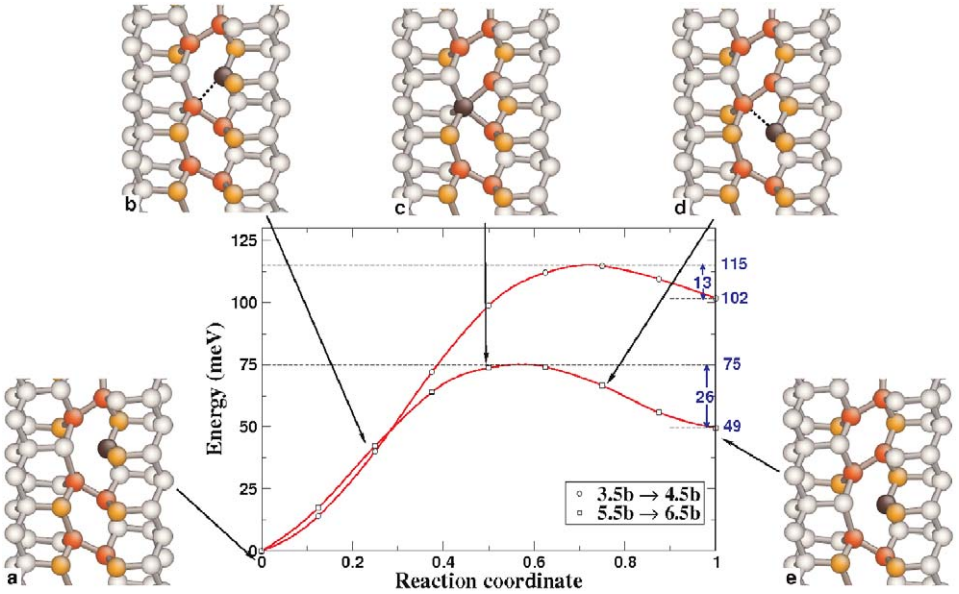

Fig. 26. NEB calculation of excess energy versus reaction coordinate (middle graph) corresponding to the migration of one kink, for two different kink–kink separations, and ball and stick representations of the successive structures (a) to (e) for a separation varying from 5.5*b* to 6.5*b*. After Pizzagalli et al. [106].

narrow kink configuration. During migration, an intermediate stable configuration including three 5-coordinated atoms is formed [106]. However, this migration mechanism appears globally close to the previous ones, with a low associated energy barrier W_m of about 160 meV.

Another important mechanism to be determined relates to the formation of a kink pair. Its theoretical determination brings additional issues, compared to the calculation of kink migration. In fact, it is necessary to consider a system that encompasses two kinks, with a separation distance large enough to prevent spontaneous kink recombination. First-principles NEB simulations of such a system is out of reach of computational facilities for the time being. However, this limitation vanishes for interatomic potential calculations, and the formation mechanism of a kink pair on a shuffle screw dislocation was investigated using both EDIP [106] and the Lenosky potential [107]. In both cases, the results show that the formation occurred following a sequence of structural rearrangements involving the breaking and formation of several bonds. Obviously, the computed mechanisms are somewhat different since the most stable configuration for a kink is different with EDIP and the Lenosky potential. However, the calculated energy barriers for the formation of a kink pair of width 3*b* are in very good agreement, with 1.25 eV for EDIP and 1.19 eV for the Lenosky potential.

Besides thermal activation, the second parameter to take into account for understanding dislocation mobility is stress. In fact, non-dissociated perfect

dislocations are observed in the low temperature, high-stress regime. Large shear stresses, estimated to about one to several GPa, are then required for displacing dislocations. This is very different from the situation occurring for partial dislocations, where thermal activation is the key factor. Despite its importance, very few investigations focused on the effect of the shear stress on kink formation and migration. The only study again concerns the shuffle screw dislocation [106]. The effect of the shear stress on the formation and migration of kinks was computed using the EDIP potential. Fig. 27 represents the energy variation due to the formation and subsequent separation of a kink pair on a perfect shuffle screw for an increasing shear strain. The repeating patterns clearly visible on each curve correspond to the energy variations due to the kink migration. Neglecting the migration, the energy variation as a function of the kink–kink distance d and the shear strain can be fitted by the following elastic expression [12]:

$$\Delta E = -\frac{K}{d} + 2F_{\mathrm{k}} - \tau bhd, \tag{6}$$

where K is an elastic coefficient, h the height of one kink, and τ is the applied shear stress. In case of no applied strain, the energy increases continuously toward the asymptotic value $2F_{\mathrm{k}}$. As expected, a shear stress is required to decrease the energy

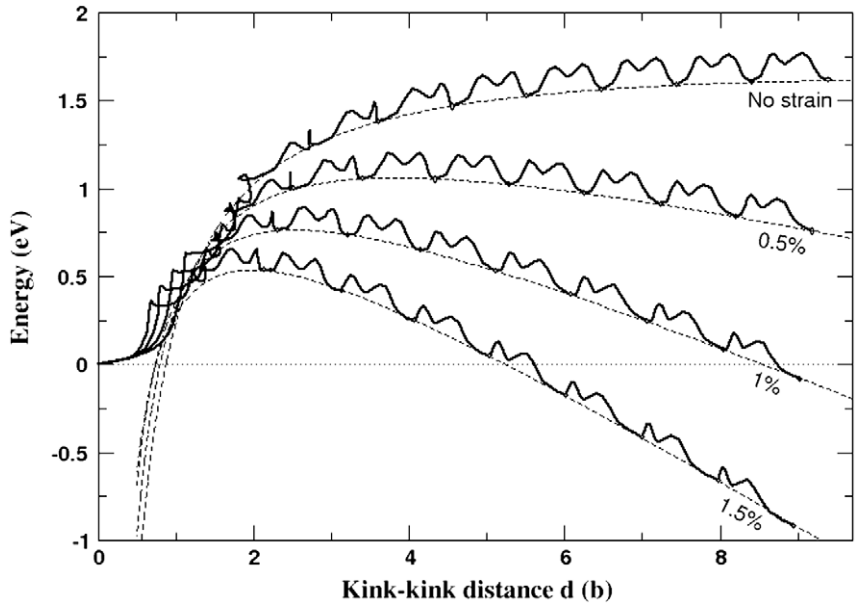

Fig. 27. Kink pair energy as a function of the kink–kink separation d (in Burgers vector unit) for various shear strain values (full lines). Fits from elasticity theory are reported as dashed lines. After Pizzagalli et al. [106].

and for preventing the spontaneous recombination of the two formed kinks. More importantly, the energy barrier to the formation of the stable kink pair, that is the maximum energy on each curve, is strongly dependent on the shear strain. Accurate determinations, taking into account the additional energy barrier due to migration, yield energy barriers of 1.20 eV for a strain of 0.5% (i.e., about 0.28 GPa) and only 0.65 eV for 1.5% (i.e., about 0.85 GPa) [106]. The last value is low enough to suggest that, in silicon, shuffle screw dislocations should be mobile in the range of low temperatures and high stresses involved in the deformation experiments reported in Section 2.

3.2.2.3. Mobility of 60° dislocations. As far as we know, there is little information available regarding the mobility of the various 60° dislocation cores represented in Fig. 22. Using the Stillinger–Weber potential, Li et al. determined a Peierls stress of approximately 1 GPa for the S_1 core [95], confirming that the 60° dislocation is more mobile than the screw dislocation. However, additional investigations of the structural and mobility properties of the 60° dislocation would be welcome. Both core configurations appear to be less mobile than S_1 and additional calculations are needed for a better understanding of the competition between core stability and mobility.

3.2.3. Effect of pressure on the core structure of perfect dislocations

Because perfect dislocations are observed in high-stress conditions where a hydrostatic component is present in the stress tensor, it is of interest to check the effect of such a hydrostatic pressure on their core structure configuration and mobility. One can expect three kinds of effects due to pressure: (i) the material is usually stiffer (this is the case for silicon), with an increase of elastic constants that affect the strain field around the core, (ii) the core structure and its stability could be modified, and (iii) pressure could favor dislocation core mobility along certain directions. One may then wonder whether theoretical investigations of non-dissociated perfect dislocations are really representative of experiments.

One first step toward an improved modeling would consist in taking into account an applied pressure. To our knowledge, there were few investigations of pressure influence on dislocation core properties. Durinck et al. [109] determined how pressure would modify the Peierls stress in olivine, an important compound for geophysicists. These authors showed that in the presence of a pressure of 10 GPa, some slip systems would harden whereas others would become softer, a result that cannot be fully explained by elastic effects. Pressure effects were also considered in the case of screw dislocation in bcc metals such as tantalum ([110]; see also Chapter 92 by Yang et al. in the present volume). It was shown that the structure of a screw dislocation core could be significantly modified upon the application of a 10 MPa pressure. However, no pressure dependence of the Peierls stress, scaled by the shear modulus, was found. Regarding semiconductors, Umeno and Černý [111] recently computed the theoretical shear stress as a function of an applied pressure in diamond, silicon, germanium, and two different silicon carbide polytypes, using first-principles calculations. These authors showed that in silicon, the ideal shear

strength is decreased by compression. This finding cannot be understood with a simple hard-sphere model, for which compression results in the squeezing of the spheres and a larger resistance against shear, a picture well suited for metals.

Recently, we investigated the effect of an applied pressure on the stability and mobility properties of the non-dissociated screw dislocation in silicon [94]. A given pressure is applied by homogeneously straining computational cells before the system is relaxed and core energies are calculated. The variations of core energies for two stable core configurations, the glide C_2 and the shuffle A, are shown in Fig. 28. While the presence of an applied pressure tends to increase the core energy of C_2, it lowers the A core energy. This result indicates that pressure can have either a positive or a negative impact on dislocation stability. It is very tempting to interpret these variations in view of an analysis of the core geometry. In fact, the A configuration is characterized by four largely stretched and distorted bonds. Applying a pressure brings atoms closer together, thus lowering the amplitude of bond stretch and distortion, which decreases the core energy. This would mean that under zero pressure conditions, the shuffle A core is in a tensile state. However, it is difficult to understand why pressure tends to increase the core energy of the C_2 configuration simply in terms of the core geometry. As a consequence, the effect of

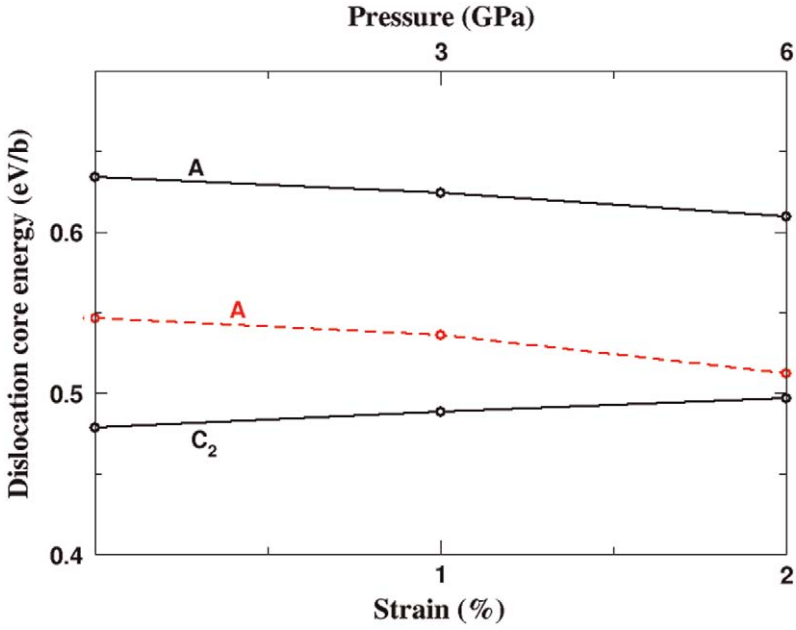

Fig. 28. Dislocation core energies of a screw dislocation as a function of an applied pressure, for shuffle A and glide C_2 cores. Values were determined from tight-binding DFTB (full lines) and DFT-GGA (dashed line) calculations, assuming that the core radius is equal to one Burgers vector *b*. After Pizzagalli et al. [94].

pressure on dislocation core stability is hardly predictable using simple arguments and atomistic calculations are mandatory for its determination.

The pressure tends to favor the shuffle core A for the screw dislocation. However, it remains energetically less favorable than the glide core C_2. Assuming that core energies vary linearly as a function of pressure, one expects a phase transition for an applied strain of about 7%, that is, a pressure of 20 GPa. This is much higher than the pressure corresponding to the phase transition from the cubic-diamond to the β-tin structure, suggesting that the glide core C_2 is the most stable configuration in all the available pressure ranges.

The core energy determination as a function of pressure requires a careful treatment. In the case of dislocation calculations using periodic boundary conditions, the total energy E of the relaxed system including N dislocations can be written

$$E = E_{\text{bulk}} + E_{\text{inter}} + NE_{\text{c}}, \tag{7}$$

where E_{bulk} is the total energy of the same system but with no dislocations, E_{inter} the interaction energy between dislocations, and E_{c} the core energy of a single dislocation. E, E_{bulk}, and E_{inter} all depend on pressure, and have to be correctly determined for an accurate calculation of E_{c}. The largest part of the energy increases in E and E_{bulk} is due to the applied strain. Both terms are obtained using systems with same geometry, thus leading to the cancellation of errors associated with total energy calculations. The last term, E_{inter}, is usually computed in the framework of anisotropic elasticity theory. In the presence of pressure, one has to consider that (i) interactions between dislocations are modified due to the reduction of distances between them and (ii) the elastic constants change as a function of pressure. E_{inter} has to be computed with the appropriate corrections, otherwise errors in core energies variations can be dramatically large [94].

The influence of an applied pressure on the mobility of the core of the non-dissociated screw dislocation was recently studied. Two possible paths were considered: (i) along a $\langle 1\,1\,2 \rangle$ direction for which the dislocation moves in $\{1\,1\,1\}$ shuffle planes and visits alternatively A and B configurations and (ii) along $\langle 1\,1\,0 \rangle$, the dislocation moving in a $\{0\,0\,1\}$ plane and passing through A and C_1 configurations. The dislocation core mobility was determined from computations of energy barriers for cores displacement along the selected directions, using the approach described in Section 3.2.2. The results reported in Fig. 29 show two opposite behaviors. For the first displacement direction, along ABA, an applied pressure leads to a progressive reduction of the Peierls energy. Conversely, the other displacement direction along ACA is increasingly energetically expensive. Therefore, this result indicates that for a given dislocation, slip directions could be hardened or softened in the presence of pressure. As for dislocation core stability, it is difficult to predict whether energy barriers will increase or decrease under pressure without the help of numerical simulations.

The presence of pressure leads to a noticeable modification of the properties of dislocation cores. In fact, both the stability and the mobility of the cores are

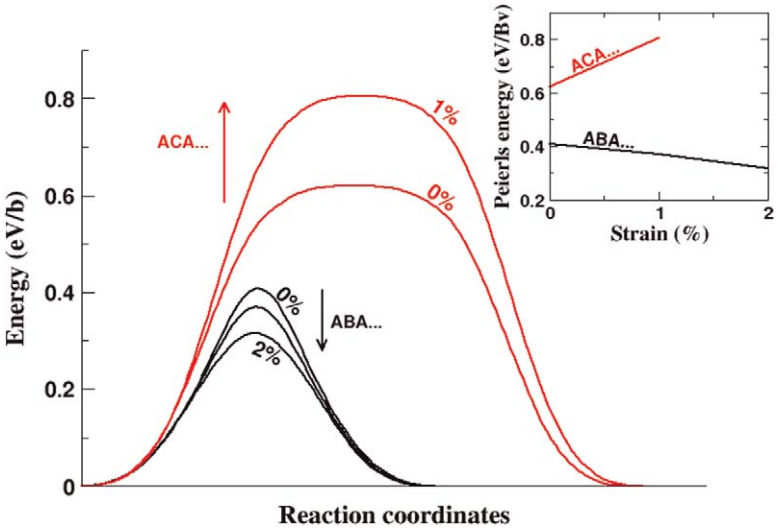

Fig. 29. Screw dislocation gliding along two different directions (see text), as a function of an applied strain. Maximum energies along the MEP are the Peierls energies; they are reported in the inset graph for clarity. After Pizzagalli et al. [94].

modified, either positively or negatively. Although silicon becomes stiffer with pressure, dislocation cores could be more mobile along specific directions. In the specific case of silicon, both the stability of the shuffle core structure A is enhanced and the dislocation displacement in shuffle planes is made easier. This is in agreement with experimental results, which suggest that dislocations are located in shuffle planes.

3.2.4. Nucleation of non-dissociated dislocations

In Section 2.2.1 we showed that in the low temperature, high-stress regime, non-dissociated dislocations were located in the neighborhood of micro-crack surface edges. Defects on these surfaces (steps, ledges) likely act as dislocation sources. Furthermore, dislocation nucleation in silicon deserves a study since there are no preexisting dislocations in virgin crystals and the nucleation and multiplication stages are the signature of macroscopic plasticity.

Compared to investigations of stability and mobility of dislocations, many fewer efforts have been devoted to nucleation. One reason is the extreme difficulty to study experimentally the onset of plasticity, essentially because of the short timescale. Nevertheless, theoretical approaches can allow one to obtain complementary information in that case. From numerical simulations focused on metals, the following conclusions were obtained [112]: (i) the formation of a dislocation from a perfect surface is very unlikely, due to a high-energy barrier and (ii) the presence of a simple defect like a step largely reduces this energy barrier by localizing stresses. Several parameters are expected to have an influence on the

nucleation mechanism, such as the structure of the surface defect (step structure, height), stress orientation, and temperature.

Regarding silicon, investigations of the possible dislocation formation from a surface step were performed by Godet et al. [96,97], from many interatomic potentials and first-principles calculations. Fig. 30 shows how a perfect 60° dislocation is nucleated from a surface step and glides in the shuffle plane passing through the step when the system is uniaxially strained by 13.6%; the stress direction is contained in the surface, at an angle of 22.5° with the step normal. The core of the dislocation is in the S_1 configuration (middle structure in Fig. 22), in agreement with the fact that 60° dislocations are supposed to be more mobile than screw dislocations. The influence of several parameters was studied, leading to the following results:

- 60° dislocations were obtained under both tension and compression, always in shuffle planes.
- No screw dislocations were nucleated.
- The latter point can be explained by considering the Schmid factors and the Peierls stresses for the screw and 60° dislocations.
- In contrast to metals, there is no localized shear in planes close to the step before the onset of plasticity.

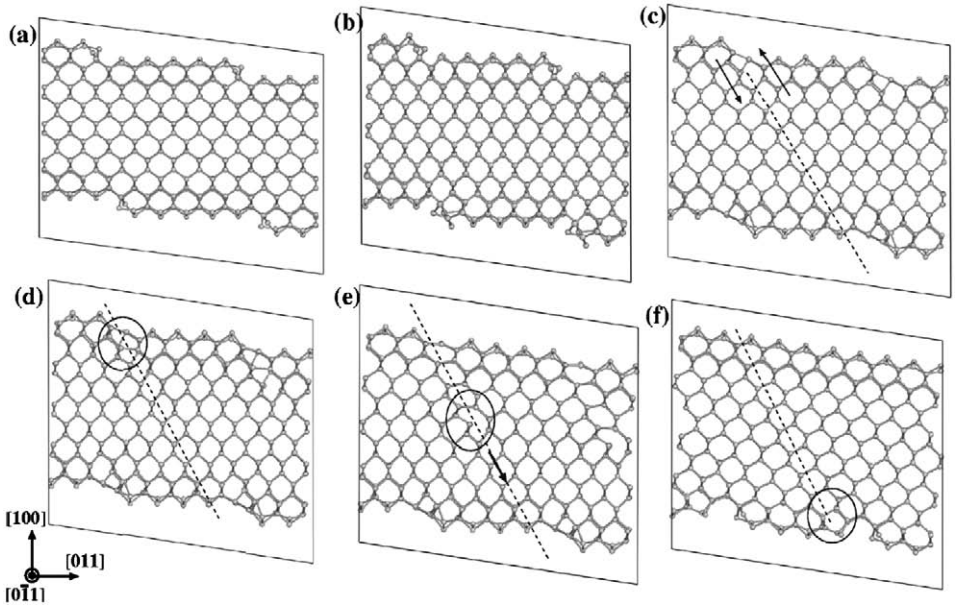

Fig. 30. Successive stages of the formation and propagation of a 60° dislocation from a strained surface, starting from a surface step. (a) Unstrained, and strains of (b) 10.4%, (c) 11.5%, and (d–f) 13.6%.

- The step geometry plays an important role on the nucleation mechanism. That the passivation of silicon surface with hydrogen prevents dislocation formation.
- Higher steps tend to make dislocation formation easier, with lower critical strains.

In the previous calculations, reduced dimensions do not allow for the 3D formation of a dislocation half-loop. This limitation was overcome by Izumi and Yip [113], who examined the nucleation mechanism of a half-loop dislocation from a sharp corner in silicon. These authors performed classical molecular dynamics simulations in high stress, low temperature conditions, which resulted in the formation and propagation in a shuffle plane of a dislocation half-loop composed of two 60° segments and one screw segment. The dislocation core structures were not described, but it is likely that the screw dislocation is in a B configuration, while a S_1 core is obtained for the 60° dislocation, since the Stillinger–Weber potential is used in this work. Configurations extracted from these simulations were then used for determining minimum energy path (MEP) with the NEB method. More recently, Godet et al. performed molecular dynamics simulations of the three-dimensional formation of a dislocation half-loop from a {1 1 1} ledge, considering different stress orientations and temperatures [114]. In the low temperature range, the outcome, shown in Fig. 31, looks very similar to the results of Izumi and Yip [113]. In fact, a half-loop located in a shuffle plane and including two 60° segments and one screw segment is obtained. The dislocation core structures are in agreement with bulk calculations.

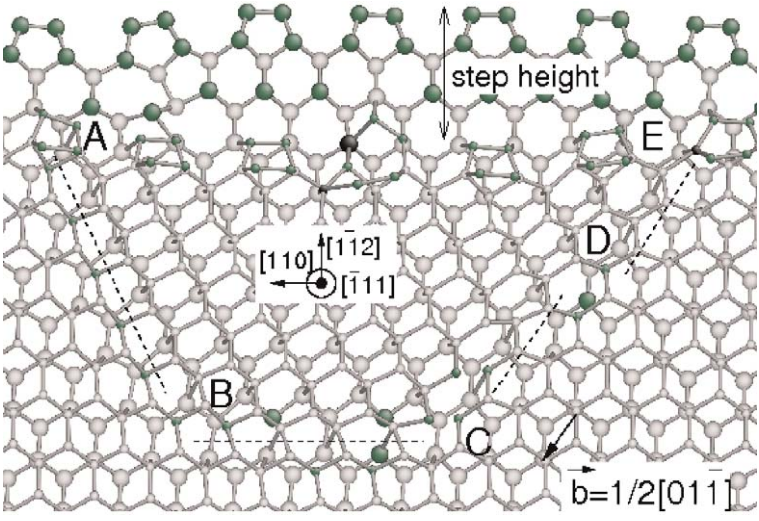

Fig. 31. Dislocation half-loop nucleated from a surface step in silicon at 600 K using the Stillinger–Weber potential. AB and BC are two 60° segments. CD and DE are two screw segments separated by a kink.

In their study, Izumi and Yip [113] indicated that the resolved shear strain for nucleation is 5.1%. In the work by Godet et al. [114], the strain value applied on the system at the onset of plasticity was 13.6%, which corresponds to a resolved shear strain of about 6.2% in the glide plane. The difference between the two values may come from the different geometry of the system, a {1 0 0} sharp corner in one case [113] and a {1 1 1} ledge in the other one [114]. Nevertheless, both values suggest that dislocation nucleation from surfaces requires large stresses, seemingly way too large compared to experimental results. However, two important points have to be considered here. First, the deformation rate in numerical simulations is several orders of magnitude higher than in experiments. It was recently shown that such a difference has a strong effect on critical stresses for dislocation nucleation [115], leading to a reduction by 50% at 300 K. Second, in numerical simulations, the dimensions of the considered systems are at best of several tens of nanometers. At this scale, it was shown experimentally in the case of nanowires and nanopillars that plasticity processes involve stresses substantially larger than in bulk materials.

4. Discussion

Recent experiments reported in Section 2 showed that, in silicon, perfect dislocations control plastic deformation at high stress. Fingerprints of such a regime were also found in some early experimental publications. This evidence motivated theoretical works using atomistic computations, reported in Section 3, in order to sort out core configurations and other properties of such perfect dislocations. The results of these two approaches are compared in this part in order to obtain a comprehensive view of this deformation regime. The transition between this regime and the other one ruled by dissociated dislocations is also discussed, together with the actual location of the dislocation cores.

Results obtained on other semiconductors are finally mentioned for discussing whether a plastic deformation regime controlled by perfect dislocations is a generic property of diamond-cubic semiconductors.

4.1. Summary of experimental and numerical results

4.1.1. Results

What was learnt from both experiments and calculations can be summarized as follows:

1. Non-dissociated dislocations clearly play an important role in the plastic deformation of silicon at low temperature, as shown by many high-stress experiments. This includes deformation experiments under a confinement pressure greater than 1.5 GPa, and scratch and indentation tests. Signatures of such dislocations can also be found during micromachining of silicon surfaces. This regime is definitely different from the high temperature one, where dislocations are dissociated and move under low applied stresses. The stress

required for displacing or nucleating non-dissociated dislocations is estimated to be larger than 1 GPa at room temperature.

2. These non-dissociated dislocations are characterized by $a/2\langle 1\,1\,0\rangle$ Burgers vectors and glide in {1 1 1} planes. Several kinds of dislocations were observed. Typical characters are 30°, 41°, and screw, but short 60° segments were also reported. In one experiment, wavy dislocations, exhibiting an average screw orientation, were found to be constituted of short 41° segments. Very little else is known about the physical signatures of these dislocations, although a few works suggest that these signatures are convoluted with those of point defects.
3. Apparently, partial dislocations obtained by high temperature deformation cannot be transformed into perfect dislocations. Conversely, the transformation of perfect dislocations into dissociated dislocations was observed, but only at a limited rate and in specific regions.
4. There exist several possible stable structures for both the screw and 60° non-dissociated cores, which are located in either glide or shuffle set planes. Glide set configurations seem to have the lowest energies in both cases. No information is available regarding the atomic structure of the 30° and 41° dislocation cores.
5. Regarding mobility, most of the available data concern the non-dissociated screw dislocation. The Peierls stress is known to be 4 and 6 GPa for the shuffle and glide cores, respectively. In the presence of an applied pressure, the mobility of the shuffle screw dislocation is enhanced. From the investigation of kink formation, one expects thermal activation to play a nonnegligible role in the mobility of the shuffle screw dislocation in the high stress, low temperature regime. For the 60° dislocation, the Peierls stress is estimated to be about 1 GPa for the shuffle core, while the undissociated glide core is not glissile.
6. Non-dissociated dislocations can be nucleated from surfaces in the shuffle set under high-stress conditions. The dislocation that is formed the most easily has a 60° orientation. Conversely, at high temperature, partial dislocations are obtained.

Usually, experiments and numerical simulations are rather complementary and it may be difficult to make meaningful comparisons. Nevertheless, there are two cases where this can be done. The first one is related to the mobility of non-dissociated dislocations. The computed Peierls stress for the non-dissociated shuffle screw dislocation is 4 GPa, in good agreement with the order of magnitude of the extrapolation at 0 K of flow stress measurements below 300 °C (Section 2.3.2). In addition, the extrapolation at 0 K of yield stress measurements performed in the medium temperature range fits quite well the computed values of the Peierls stress for glide dislocations. Numerical simulations revealed that the thermally activated motion of non-dissociated screw dislocations was possible at 300 °C under an applied stress of 1.5 GPa, as reported from yield stress measurements (Section 2.3.2). The second case concerns the nucleation of dislocations. Molecular dynamics simulations of the dislocation nucleation from surface steps

suggest that the two types of dislocations, partial or non-dissociated ones, can be generated depending on the applied stress and temperature. This defines two regimes, in agreement with experimental findings.

4.1.2. Current limitations

In spite of numerous studies dedicated to non-dissociated dislocations, there are still many open issues. In fact, there are several limitations to both experiments and numerical simulations, which tend to hinder progress in this domain. Regarding experiments, several limitations are either intrinsic to the techniques or due to the specificity of deformation experiments. First, dislocation observations are performed *postmortem*. Therefore, one may wonder whether the dislocations participating in plastic flow do not experience some modifications before being observed by TEM. In other words, are the dislocations at rest the same as the moving dislocations? *In situ* experiments seem difficult to perform because of complications associated with high-stress requirements. Secondly, although atomic-scale resolution can be achieved by TEM, the determination of the atomic structure of dislocation cores is hardly feasible in silicon using this technique. Finally, non-dissociated dislocations are obtained in a high-stress regime, which usually results in highly damaged samples, containing cracks, point defects, and various micro-structural defects. This makes the analysis all the more difficult.

Numerical simulations suffer from other limitations. Accurate first-principles calculations are very limited in size, as they include usually only a few hundreds of atoms. Given the complexity of dislocation cores and the associated long-range stress fields, first-principles calculations are then restricted to infinite straight dislocations, or to very simple defects along the dislocation lines. Moreover, calculations are essentially static, because computational costs prevent performing dynamical simulations. Another option is the use of classical interatomic potentials, which allow simulating large systems and performing dynamical studies. This provides a way for investigating realistic situations like the thermally activated propagation of curved dislocation segments. However, the reliability of the obtained results is questionable because of the inability of the available potentials for silicon to model reconstructed cores accurately. Tight-binding calculations could be a third viable option, with a good accuracy and a considerable speedup compared to first-principles methods.

4.2. Transition between two regimes: a core structure transformation?

The calculations of Duesbery and Joós [45] fed most of the interpretations about the existence of perfect dislocations at high stress in silicon. This regime can be explained by the fact that perfect shuffle dislocations are the more mobile ones at high stresses. These calculations rely upon dislocation modeling with the Peierls–Nabarro model, using as input gamma surfaces calculated from atomistic computations. Yet, the position of the transition stress is very sensitive to the gamma surface input and to the assumed shape of the kink pairs. Thus, these

calculations cannot be considered as giving reliable transition stress values (P. Carrez, private communication). Furthermore, recent atomistic calculations [116,117] show that a perfect shuffle screw is more mobile than a 30° glide partial in the whole range of stresses. This makes questionable the hypothesis of an intrinsic mechanism responsible for such a transition, unless the mobility of perfect $\langle 1\,1\,2 \rangle$/30° dislocations has to be considered instead that of the screw ones.

Extrinsic factors could also be put forward to explain this transition. Indeed, experimental observations show numerous pinning points on perfect dislocations, whose density increases with temperature. Such pinning points could slow down progressively perfect dislocations to the benefit of partial dislocations.

A point to be clarified is whether the nucleation of partial glide dislocations is assisted when perfect shuffle dislocations preexist. Then, one would have to consider possible mechanisms for core transformation.

The core of PS and DG dislocations can be transformed from one to the other through several elementary mechanisms. The two basic mechanisms that allow dislocations moving over one atomic distance to switch from one set to the other are cross slip and climb (Fig. 32). Some mechanisms that can be involved in such transformations are similar to those proposed in the frame of composite models of dislocation core structures, in which a dissociated dislocation can "move" from glide set to shuffle set in its dissociated form (see, e.g., [1]). However, in composite models, the transformation mechanisms are relevant to the movement of partial dislocations from glide to shuffle positions and a constriction of the parent dislocations is not required. In the present case, the transformation mechanism concerns the change from perfect to dissociated dislocations (as well as the reverse transformation), and a different mechanism can also be involved, namely cross slip [57].

Mechanisms involving the nucleation of fresh dislocations in the stress field of dislocations of another type can also be considered but will not be discussed here.

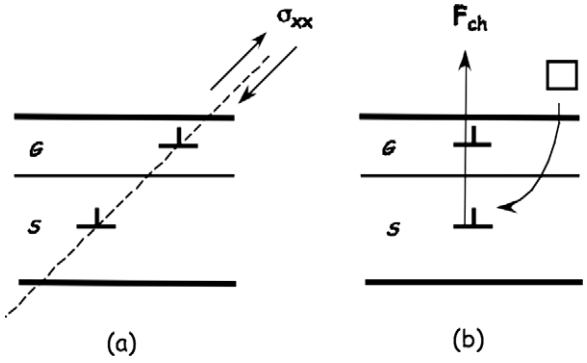

Fig. 32. Transformation from a perfect shuffle dislocation into a dissociated glide dislocation. The perfect dislocation has moved by one interplanar spacing into the glide set by: (a) stress-assisted (shear stress σ_{jj}) cross slip and (b) climb under the action of a chemical force (F_{ch}). After Rabier [86].

Cross slip is a conservative mechanism that occurs under stress with the help of thermal activation. Climb requires point defect annihilations at the dislocation cores and can also be stress-assisted, but to a lesser extent. This indicates that cross slip can be operative at lower temperatures than climb, and points at the core structure of perfect screw dislocations as an important factor determining the stability of perfect shuffle dislocations.

Cross slip is initiated when a critical part of the parent dislocation deviates in the cross slip plane. If the parent dislocation is a perfect one, this can be achieved through local stress concentrations. In the case of a dissociated dislocation, a local constriction of the stacking-fault ribbon is required in a first step to allow for a deviation. Thus, cross slip may be easier from PS to DG than from DG to PS.

Dislocation climb proceeds by point defect absorption or emission at jogs. In the same way, climb mechanisms, which allow transforming a DG into a PS, are less efficient in the presence of a stacking fault. However, point defect absorption can take place either on a preexisting constriction or on one of the glide partials, transforming it into a partial located in the shuffle plane. In this last case, this can help forming a constriction. As compared to previous mechanisms, the transformation PS–DG is trivial: a PS segment climbs over one atomic distance into the glide set; it can then dissociate and form a DG segment.

Thus, mechanisms allowing the transformation from dissociated glide dislocations to perfect shuffle ones are possibly more difficult than the reverse ones. The results of atomistic computations reported in Section 3.2.2 show that it is impossible to move a perfect shuffle dislocation out of its glide plane under the action of a shear stress. Hence, cross slip cannot be considered as a viable mechanism to move a screw dislocation from the shuffle set to the glide set. A climb mechanism is then expected for such a transformation, but it requires a sufficient point defect mobility and concentration.

What was described above about core transformations is relevant to a change of the location of a perfect dislocation core from the shuffle set to the glide set. Another subsequent limiting factor in obtaining a dissociated dislocation in the glide set could be the dissociation process itself. Indeed, starting from a perfect dislocation in the glide set, the incipient partial dislocations are submitted to a Peierls stress in the dissociation (slip) plane. This Peierls stress can be so large as to prevent any gain in elastic energy during the splitting process, unless thermal activation assists the motion of the partial dislocations. Takeuchi [118,119] calculated that a Peierls stress on partial dislocations of the order of 0.02μ to 0.04μ, which is realistic in the case of silicon, could prevent dissociation in the absence of thermal activation.

Following the conclusions of Takeuchi, one may ask whether the transition from a perfect to a dissociated core in silicon could be relevant to the dissociation of a perfect dislocation located in the glide set, which dissociates as soon as temperature and stress allow for the partial dislocations to move. This hypothesis can be ruled out, however, on the basis of the atomistic calculations on dislocation nucleation (Section 3.2.4), where dislocations were found to be nucleated as perfect ones in the shuffle set at high stress and in a dissociated form in the glide set at high temperature.

Are they two different and independent deformation microstructures depending on the thermomechanical conditions? Experimentally, no massive transformation was evidenced from preexisting perfect dislocations to dissociated ones. The interpretations proposed by Rabier and Demenet [69] and Saka et al. [76] seem to be very different, that is, there is no transformation but nucleation of dissociated dislocations, apparently with no relation to preexisting perfect defects [69], or there is a core transformation [76]. The two experiments were performed in very different conditions, but a common interpretation could be that a small critical nucleus of transformed core can provide a source for a new dislocation population [86], leaving unaffected most of the parent dislocation microstructure.

4.3. Are non-dissociated dislocations in the glide or the shuffle set?

Since the pioneering works of Shockley [9] and Hornstra [10], it was always assumed that non-dissociated dislocations would have a shuffle core. In fact, it appeared easier (and less energetically expensive) to break a single bond to form a shuffle core than to break three bonds to form a glide core. However, we know that the covalent nature of silicon bonding tends to favor reconstruction, as is the case for partial dislocation cores. Thus, one may wonder whether the early assumption is still valid in the view of recent results. Considering experimental observations first, it is extremely difficult to reach certainty on this matter although, in principle, it could be possible to perform direct observations of dislocation cores at the atomic-scale level, using for instance corrected HREM.

Numerical simulations should be more appropriate for determining the core structures. All calculations suggest that for screw and 60° orientations, the most stable dislocation cores exhibit a glide character. However, considering first the screw dislocation, the Peierls stress of the reconstructed glide core is 50% larger than that of the shuffle core. Also, due to reconstruction, the kink migration energy is likely to be higher for the glide core than for the shuffle one. Therefore, the glide screw dislocation is expected to be less mobile than the shuffle core, and one may wonder whether the most stable dislocation cores are those that really matter for plastic deformation. This issue is even more critical in the case of the 60° dislocation. The glide core appears to be much more stable than the shuffle core, but it is sessile with a very high Peierls stress. Atomistic simulations also raise another point. The denominations shuffle or glide are related to the type of {1 1 1} plane the center of the dislocation core is located in. In the case of a dislocation core with a complex reconstructed structure, or encompassing two adjacent {1 1 1} planes (see, for instance, the core S_3 for the 60° dislocation), it might be difficult to settle the question in terms of shuffle or glide.

4.4. Other semiconductor materials

From the results obtained about perfect dislocations at high stress in silicon, the question arises of whether this feature is specific to silicon or is generic to

semiconductor materials. As far as the ductile to brittle transition is concerned, the macroscopic behavior of most semiconductors is analogous to that of silicon. This transition was experimentally observed and analyzed on several materials such as, for instance, GaAs [120] and SiC [121]. High-stress microstructures were studied in III–V compounds (GaAs, InSb, InP, …) and in group IV materials.

Using a solid confining pressure of 1.2 GPa, it was possible to extend the usual plastic domain of plasticity and to deform GaAs, InP, and InSb down to 77 K [122]. This increase in the investigated plastic range led to the observation of a hump in the stress versus temperature curves. Furthermore, a transition appeared clearly in a plot of the logarithm of the resolved shear stress as a function of the inverse of temperature. The microstructures, which consisted mainly of perfect screw dislocations below the transition temperature, were interpreted as resulting from a glide to shuffle transition. However, no calculations have been done yet in III–V compounds to confirm the occurrence of this transition. Very recently, indentations on InSb were performed both at room and liquid nitrogen temperatures by Kedjar [123] and Kedjar et al. [124]. At room temperature, the microstructure is made up of partial dislocations, while at 77 K it is made up of perfect screw dislocations. However, no segment was found lying along the $\langle 1\,1\,2 \rangle$ or $\langle 1\,2\,3 \rangle$ directions. This is in agreement with results presented in Ref. [122]. The case of III–V compounds appears to be close to that of silicon, but with some differences in the dislocation microstructures at high stress.

Compression tests at constant strain rate were conducted on 6H- and 4H-SiC, two of the most common polytypes of this material; the plot of the logarithm of the resolved shear stress as a function of the inverse of temperature exhibits a transition associated with two well-defined microstructures [125,126]. At high temperature, dislocations are dissociated into leading-trailing pairs of partials, whereas at low temperature only the leading partial with silicon core is observed together with its associated stacking fault. Other observations on 4H-SiC deformed under a confining pressure of 5 GPa at room temperature and 150 °C, using an anisotropic multi-anvil apparatus, show that the microstructure is composed of both widely dissociated dislocations and undissociated perfect dislocations [127]. The very high density of dislocations after deformation prevented making a fine analysis of the microstructure. It would be of interest to perform high-stress experiments on cubic silicon carbide, which is now available in bulk dimensions.

In Ref. [93], the authors examined the various possible configurations of a perfect screw dislocation in group IV materials by means of first-principles calculations. It appears that the stable screw dislocation is located in the shuffle set for Ge and in the glide set for diamond. No experimental observations were reported yet in Ge. Preliminary experiments on diamond deformed under a pressure of 5 GPa in a multi-anvil apparatus show a high density of dislocations without apparent dissociation, but this result has to be confirmed [128]. In addition, in plastically deformed natural type IIa brown diamonds after high pressure, high temperature annealing, Blumenau et al. [129] found that although most 60° dislocations are found to be dissociated, some appear to be undissociated. This is providing evidence of the existence of two types of dislocations cores.

In conclusion, several semiconductors exhibit the same behavior as silicon under very high stress. This could be a general feature for all semiconducting materials, but with specificities for each material depending on the structure and the covalent versus ionicity balance of the bonding.

4.5. Perspectives

Regarding the issue of glide versus shuffle dislocation cores, experiments are needed to determine the exact location of the perfect dislocations and to establish a correlation between their actual core structures and their physical properties. The investigation of the core structure of dislocations has to be performed using corrected HREM. Clearly, the main difficulty arises from the preparation of an adequate specimen with edge-on dislocations, whose core is not affected by kinks, impurities, or any defect that may blur the structure determination. As far as electron microscopy is concerned, *in situ* nanoindentation experiments can be useful provided this technique can be extended down to atomic scale. This is a technical challenge.

Spatially resolved photoluminescence could help understanding the shuffle–glide transition since it was shown that perfect dislocations have different signatures than dissociated glide dislocations. It would be interesting to follow locally the change in signature of dislocations and, in particular, to check whether some transient core structures or premonitory events are associated to the transition.

Currently, there is a lack of EBIC experiments devoted to the electrical properties of dislocations in silicon. Experiments such as scanning transmission electron beam induced current (STEBIC) could be used to reinvestigate these electrical properties, especially those of perfect dislocations.

EPR is a technique that has been widely used in the determination of the structure of dissociated dislocations (see Section 1.3); this technique would be of interest for determining whether dangling bonds are present in the core of a perfect dislocation.

Concerning numerical simulations, atomistic computations of $\langle 1\,1\,2\rangle/30^\circ$ and $\langle 1\,2\,3\rangle/41^\circ$ dislocations are lacking. Understanding why they are controlling the low temperature deformation microstructures is one of the key issues: the determination of their core configurations and of the structure and mobility of kinks on these dislocations is needed. Nucleation of new dislocations in the stress field of perfect dislocations should also be investigated by atomistic computations. This could shed light on the transition between the two modes of deformation in silicon. The influence of the nature and availability of nucleation sites on dislocation nucleation should also be checked.

Finally, some macroscopic properties should be revisited. As an example, the brittle to ductile transition could be investigated in the light of the existence of perfect dislocations. HREM and TEM experiments should be devoted to examine the very first steps of dislocation nucleation at crack tips. Passivation treatments

should also be used on Si samples in the range of high stress in order to check their influence on mechanical properties, as was done in the other deformation regime (see, e.g., [130]). This could provide information on dislocation mobility as well as on the issue of dangling bonds within the core of perfect dislocation. Finally, the transition between perfect and dissociated dislocations could be reinvestigated by determining the influence of stress and temperature.

4.6. Concluding remarks

In 1996, in their paper dedicated to the mobility of dislocations in silicon, Duesbery and Joós [45] stated that: "Theoretical arguments, without exception, predict that slip should occur on the shuffle planes. With equal unanimity experimental observations indicate that slip does occur on the glide planes." However, a review of the scientific literature clearly indicates that perfect dislocations exist at high stress, bringing back consistency to the former theoretical analyses of the 1950s. Following this argument, the perfect dislocations should glide on the shuffle set planes. Although indirect evidence exists to support this hypothesis, the current state of knowledge does not allow one to draw a clear and definite conclusion on this last point. More has to be done to understand the actual core structure of dislocations in silicon, and the transition between high- and low-stress deformation regimes.

References

[1] H. Alexander, in: F.R.N. Nabarro (Ed.), Dislocations in Solids, vol. 7, North-Holland, Amsterdam, 1986, p. 115.
[2] A. George, J. Rabier, Rev. Phys. Appl. 22 (1987) 941.
[3] J. Rabier, A. George, Rev. Phys. Appl. 22 (1987) 1327.
[4] H. Alexander, H. Teichler, Electronic structure and properties of semiconductors, in: P. Haasen, W. Schröter (Eds.), Materials Science and Technology, vol. 4, 1991, p. 249.
[5] T. Figielski, J. Phys. Condens. Matter 14 (2002) 12665.
[6] D.B. Holt, B.G. Yacobi, Extended Defects in Semiconductors, Cambridge University Press, UK, 2007.
[7] C.J. Gallagher, Phys. Rev. 88 (1952) 721.
[8] F. Seitz, Phys. Rev. 88 (1952) 722.
[9] W. Shockley, Phys. Rev. 91 (1953) 228.
[10] J. Hornstra, J. Phys. Chem. Solids 5 (1958) 129.
[11] P. Haasen, A. Seeger, in: W. Schottky (Ed.), Halbleiterprobleme, vol. IV, Vieweg, Wiesbaden, 1958, p. 68.
[12] J.P. Hirth, J. Lothe, Theory of Dislocations, first ed., MacGraw-Hill, New York, 1968; id. Theory of Dislocations, second ed., MacGraw-Hill, New York, 1982.
[13] W.C. Dash, J. Appl. Phys. 27 (1956) 1193; 31 (1960) 2275.
[14] K. Wessel, H. Alexander, Phil. Mag. 35 (1977) 1523.
[15] H. Alexander, J. Phys. Coll. C7 (1974) 173.
[16] S. Amelinckx, in: F.R.N. Nabarro (Ed.), Dislocations in Solids, vol. 2, North-Holland, Amsterdam, 1979, p. 67.
[17] D.J.H. Cockayne, I.L.F. Ray, M.J. Wheelan, Phil. Mag. A 20 (1969) 1265.

[18] I.L.F. Ray, D.J.H. Cockayne, Phil. Mag. 22 (1970) 853.
[19] I.L.F. Ray, D.J.H. Cockayne, Proc. R. Soc. A 325 (1971) 543.
[20] E. Aerts, P. Delavignette, R. Siems, A. Amelinckx, J. Appl. Phys. 33 (1962) 3078.
[21] R. Meingast, H. Alexander, Phys. Stat. Sol. (a) 17 (1973) 229.
[22] G. Packeiser, P. Haasen, Phil. Mag. 35 (1977) 821.
[23] G. Packeiser, Phil. Mag. A 41 (1980) 459.
[24] F. Louchet, J. Thibault-Desseaux, Rev. Phys. Appl. 22 (1987) 207.
[25] H. Alexander, R. Labusch, W. Sander, Solid State Commun. 3 (1965) 357.
[26] E. Weber, H. Alexander, J. Phys. Coll. 40-C6 (1979) 101.
[27] V.A. Grazhulis, Y.A. Osipyan, Sov. Phys. JETP 31 (1970) 677Sov. Phys. JETP 33 (1971) 623.
[28] V.G. Eremenko, E. Yakimov, N. Abrosimov, Phys. Stat. Sol. (c) 4 (2007) 3100.
[29] P.B. Hirsch, J. Phys. Coll. 40-C6 (1979) 27.
[30] R. Jones, J. Phys. Coll. 40-C6 (1979) 33.
[31] J. Bennetto, R.W. Nunes, D. Vanderbilt, Phys. Rev. Lett. 79 (1997) 245.
[32] W. Cai, V.V. Bulatov, J. Chang, J. Li, S. Yip, in: F.R.N. Nabarro, J.P. Hirth (Eds.), Dislocations in Solids, vol. 12, North-Holland, Amsterdam, 2004, p. 1.
[33] V.V. Bulatov, S. Yip, A.S. Argon, Phil. Mag. A 72 (1995) 453.
[34] R. Jones, J. Phys. Coll. 44-C4 (1983) 61.
[35] M. Heggie, R. Jones, Phil. Mag. B 48 (1983) 365.
[36] H.J. Möller, U. Jenrich, in: R. Tressler, R. Bradt (Eds.), Deformation of Ceramic Materials, Plenum Press, New York, 1984, p. 25.
[37] P. Gadaud, J. Woirgard, P. Mazot, J.L. Demenet, J. de Fouquet, J. Phys. Coll. 48-C8 (1987) 101.
[38] B.Ya. Farber, Yu.L. Iunin, V.I. Nikitenko, Phys. Stat. Sol. (a) 97 (1986) 469.
[39] P.B. Hirsch, A. Ourmazd, P. Pirouz, Inst. Phys. Conf. Ser. 60 (1981) 29.
[40] F. Louchet, Phil. Mag. A 43 (1981) 1289.
[41] H. Alexander, J.C.H. Spence, D. Shindo, H. Gottschalk, N. Long, Phil. Mag. A 53 (1986) 627.
[42] H.R. Kolar, J.C.H. Spence, H. Alexander, Phys. Rev. Lett. 77 (1996) 4031.
[43] R. Jones, Phil. Mag. B 42 (1980) 213.
[44] K. Maeda, Y. Yamashita, Phys. Stat. Sol. (a) 138 (1993) 523.
[45] M.S. Duesbery, B. Joós, Phil. Mag. Lett. 74 (1996) 253.
[46] J. Samuels, S.G. Roberts, Proc. R. Soc. Lond. A 421 (1989) 1.
[47] P.B. Hirsch, S.G. Roberts, Phil. Mag. 64 (1991) 55.
[48] B. Moser, K. Wasmer, L. Barbieri, J. Michler, J. Mater. Res. 22 (2007) 1004.
[49] S. Minomura, H.G. Drickamer, J. Phys. Chem. Solids 23 (1962) 451.
[50] I.V. Gridneva, Yu.V. Milman, V.I. Trefilov, Phys. Stat. Sol. (a) 14 (1972) 177.
[51] T. Suzuki, T. Ohmura, Phil. Mag. A 74 (1996) 1073.
[52] V.G. Eremenko, V.I. Nikitenko, Phys. Stat. Sol. (a) 14 (1972) 317.
[53] M.J. Hill, D.J. Rowcliffe, J. Mater. Sci. 9 (1974) 1569.
[54] J. Castaing, P. Veyssière, L.P. Kubin, J. Rabier, Phil. Mag. A 44 (1981) 1407.
[55] J.L. Demenet, Thèse d'Etat, Université de Poitiers, France, 1987.
[56] M. Cagnon, in: Les Editions de Physique (Ed.), Dislocations et Déformation Plastique, Orsay, 1980, p. 55.
[57] J. Rabier, J.L. Demenet, Phys. Stat. Sol. (b) 222 (2000) 63.
[58] J. Rabier, P. Veyssière, J.L. Demenet, J. Phys. Coll. 44-C4 (1983) 243.
[59] P. Cordier, D. Rubie, Mater. Sci. Eng. A 309–310 (2001) 38.
[60] J. Rabier, P. Cordier, J.L. Demenet, H. Garem, Mater. Sci. Eng. A 309–310 (2001) 74.
[61] J. Rabier, P. Cordier, T. Tondellier, J.L. Demenet, H. Garem, J. Phys. Condens. Matter 12 (2000) 10059.
[62] J. Rabier, M.F. Denanot, J.L. Demenet, P. Cordier, Mater. Sci. Eng. A 387–389 (2004) 124–128.
[63] A. George, G. Champier, Phys. Stat. Sol. (a) 53 (1979) 529.
[64] B. Pichaud, P. Jean, F. Minari, Phil. Mag. A 54 (1986) 479.
[65] J. Rabier, J.L. Demenet, M.F. Denanot, X. Milhet, Mater. Sci. Eng. A 400–401 (2005) 97.
[66] K. Asaoka, T. Umeda, S. Arai, H. Saka, Mater. Sci. Eng. A 400–401 (2005) 93.

[67] G. de Wit, J.S. Koelher, Phys. Rev. 116 (1959) 1113.
[68] H. Gottschalk, J. Phys. Coll. 44-C4 (1983) 69.
[69] J. Rabier, J.L. Demenet, Phys. Stat. Sol. (a) 202 (2005) 944.
[70] J.L. Demenet, J. Rabier, H. Garem, Inst. Phys. Conf. Ser. 87 (1987) 355.
[71] J. Rabier, P.O. Renault, D. Eyidi, J.L. Demenet, J. Chen, H. Couvy, L. Wang, Phys. Stat. Sol. (c) 4 (2007) 3110.
[72] Y. Wang, W.B. Durham, I.C. Getting, D.J. Weidner, Rev. Sci. Instrum. 74 (2003) 3002.
[73] M. Omri, Thèse, INPL, Nancy, France, 1981.
[74] I. Zarudi, L.C. Zhang, J. Mater. Process. Technol. 84 (1998) 149; Int. J. Mech. Sci. 43 (2001) 1985.
[75] S. Johansson, J.Å. Schweitz, K. Peter, O. Lagerlöf, J. Am. Ceram. Soc. 72 (1989) 1136.
[76] H. Saka, K. Yamamoto, S. Arai, K. Kuroda, Phil. Mag. 86 (2006) 4841.
[77] J. Rabier, J.L. Demenet, Scr. Mater. 45 (2001) 1259.
[78] A. Oueldennaoua, R. Allem, A. George, J.P. Michel, Phil. Mag. A 57 (1988) 51.
[79] P. Grosbras, J.L. Demenet, H. Garem, J.C. Desoyer, Phys. Stat. Sol. (a) 84 (1984) 481.
[80] H.S. Leipner, Z. Wang, H. Gu, V.V. Mikhnovich Jr., V. Bondarenko, R. Krause-Rehberg, J.L. Demenet, J. Rabier, Phys. Stat. Sol. (a) 201 (2004) 2021.
[81] S. Pizzini, S. Binetti, A. Le Donne, A. Marzegalli, J. Rabier, Appl. Phys. Lett. 88 (2006) 211910.
[82] N.A. Drozdov, A.A. Patrin, V.D. Tkachev, Pis'ma Zh. Eksp. Teor. Fiz. 23 (1976) 651; Sov. Phys. JETP Lett. 23 (1976) 597.
[83] E.A. Steinman, A.N. Tereshchenko, J. Rabier, Proc. 23rd Int. Conf. "The Physics of Extreme State of Matter", Elbrus, Kabardino-Balkaria, Russia, 2008.
[84] P.D. Nellist, M.F. Chisholm, N. Dellby, O.L. Krivanek, M.F. Murfitt, Z.S. Szilagyi, A.R. Lupini, A. Borisevich, W.H. Sides Jr., S.J. Pennycook, Science 305 (2004) 1741.
[85] L. Pizzagalli, P. Beauchamp, H. Jónsson, Phil. Mag. 88 (2008) 91.
[86] J. Rabier, Phys. Stat. Sol. (a) 204 (2007) 2248.
[87] K.C. Pandey, Phys. Rev. Lett. 47 (1981) 1913.
[88] G. Csànyi, T. Albaret, M.C. Payne, A. De Vita, Phys. Rev. Lett. 93 (2004) 175503.
[89] T.A. Arias, J.D. Joannopoulos, Phys. Rev. Lett. 73 (1994) 680.
[90] L. Pizzagalli, P. Beauchamp, J. Rabier, Phil. Mag. A 83 (2003) 1191.
[91] C. Wang, J. Li, K. Ho, S. Yip, Appl. Phys. Lett. 89 (2006) 051910.
[92] H. Koizumi, Y. Kamimura, T. Suzuki, Phil. Mag. A 80 (2000) 609.
[93] L. Pizzagalli, P. Beauchamp, J. Rabier, Europhys. Lett. 72 (2005) 410.
[94] L. Pizzagalli, J.L. Demenet, J. Rabier, Phys. Rev. B 79 (2009) 045203.
[95] C. Li, Q. Meng, G. Li, L. Yang, Superlatt. Microstruc. 40 (2006) 113.
[96] J. Godet, L. Pizzagalli, S. Brochard, P. Beauchamp, Phys. Rev. B 70 (2004) 054109.
[97] J. Godet, S. Brochard, L. Pizzagalli, P. Beauchamp, J.M. Soler, Phys. Rev. B 73 (2006) 092105.
[98] B. Joós, Q. Ren, M.S. Duesbery, Phys. Rev. B 50 (1994) 5890.
[99] Q. Ren, B. Joós, M.S. Duesbery, Phys. Rev. B 52 (1995) 13223.
[100] L. Pizzagalli, P. Beauchamp, Phil. Mag. Lett. 84 (2004) 729.
[101] T. Suzuki, S. Takeuchi, in: S. Takeuchi, T. Suzuki (Eds.), Lattice Defects in Ceramics, Publication Office of Jpn. J. Appl. Phys., Tokyo, 1989, p. 9.
[102] H. Koizumi, H.O.K. Kirchner, T. Suzuki, Phil. Mag. 86 (2006) 3835.
[103] H. Jónsson, G. Mills, K.W. Jacobsen, in: B.J. Berne, G. Ciccotti, D.F. Coker (Eds.), Classical and Quantum Dynamics in Condensed Phases Simulations, vol. 16, World Scientific, Singapore, 1998, p. 385.
[104] M. Miyata, T. Fujiwara, Phys. Rev. B 63 (2001) 045206.
[105] H. Koizumi, T. Suzuki, Mater. Sci. Eng. A 400–401 (2005) 76.
[106] L. Pizzagalli, A. Pedersen, A. Arnaldsson, H. Jónsson, P. Beauchamp, Phys. Rev. B 77 (2008) 064106.
[107] A. Pedersen, L. Pizzagalli, H. Jónsson, J. Phys. Condens. Matter 21 (2009) 084210.
[108] G. Henkelman, H. Jónsson, J. Chem. Phys. 111 (1999) 7010.
[109] J. Durinck, A. Legris, P. Cordier, Phys. Chem. Miner. 32 (2005) 646.
[110] L. Yang, P. Söderlind, J. Moriarty, Mater. Sci. Eng. A 309–310 (2001) 102.
[111] Y. Umeno, M. Černý, Phys. Rev. B 77 (2008) 100101(R).

[112] S. Brochard, P. Beauchamp, J. Grilhé, Phys. Rev. B 61 (2000) 8707.
[113] S. Izumi, S. Yip, J. Appl. Phys. 104 (2008) 033513.
[114] J. Godet, S. Brochard, L. Pizzagalli, J. Appl. Phys. 105 (2009) 026104.
[115] T. Zhu, J. Li, A. Samanta, A. Leach, K. Gall, Phys. Rev. Lett. 100 (2008) 025502.
[116] W. Cai, Ph.D. thesis, Massachusetts Institute of Technology, USA, 2001.
[117] L. Pizzagalli, P. Beauchamp, Phil. Mag. Lett. 88 (2008) 421.
[118] S. Takeuchi, J. Alloys Comp. 378 (2004) 61.
[119] S. Takeuchi, Mater. Sci. Eng. A 400–401 (2005) 84.
[120] S. Wang, P. Pirouz, Acta Mater. 55 (2007) 5515.
[121] M. Zhang, H.M. Hobgood, J.L. Demenet, P. Pirouz, J. Mater. Res. 18 (2003) 1087.
[122] T. Suzuki, T. Yasutomi, T. Tokuoka, I. Yonenaga, Phil. Mag. A 79 (1999) 2637.
[123] B. Kedjar, Thesis, University of Poitiers, France, 2007.
[124] B. Kedjar, L. Thilly, J.L. Demenet, J. Rabier, Mater. Res. Soc. Proc. 1026-C11 (2008) 1.
[125] A.V. Samant, P. Pirouz, Int. J. Refractory Metals Hard Mater. 16 (1998) 277.
[126] J.L. Demenet, M.H. Hong, P. Pirouz, Scr. Mater. 43 (2000) 865.
[127] J.L. Demenet, X. Milhet, J. Rabier, P. Cordier, Mater. Sci. Forum 457–460 (2004) 343.
[128] J. Rabier et al., unpublished data.
[129] A.T. Blumenau, R. Jones, T. Frauenheim, B. Willems, O.I. Lebedev, G. Van Tendeloo, Phys. Rev. B 68 (2003) 014115.
[130] Y. Yamashita, F. Jyobe, Y. Kamiura, K. Maeda, Phys. Stat. Sol. (a) 71 (1999) 27.